MIT
International Center for
Air Transportation

MODELING PERFORMANCE AND NOISE OF ADVANCED OPERATIONAL PROCEDURES FOR CURRENT AND FUTURE AIRCRAFT

Jacqueline L. Thomas and R. John Hansman

Technical Report Documentation Page

1. Report No.	2. Government Accession No.	3. Recipient's Catalog No.

4. Title and Subtitle	5. Report Date
	6. Performing Organization Code

7. Author(s)	8. Performing Organization Report No.

9. Performing Organization Name and Address	10. Work Unit No. (TRAIS)
	11. Contract or Grant No.

12. Sponsoring Agency Name and Address	13. Type of Report and Period Covered
	14. Sponsoring Agency Code

15. Supplementary Notes

16. Abstract

17. Key Words	18. Distribution Statement

19. Security Classif. (of this report)	20. Security Classif. (of this page)	21. No. of Pages	22. Price
Unclassified	Unclassified		

Form DOT F 1700.7 (8-72)   Reproduction of completed page authorized

[Page Intentionally Left Blank]

MODELING PERFORMANCE AND NOISE OF ADVANCED OPERATIONAL PROCEDURES FOR CURRENT AND FUTURE AIRCRAFT

by

Jacqueline L. Thomas and Prof. R. John Hansman

ABSTRACT

Increasing concerns regarding aircraft noise has encouraged the push to reduce noise via operational adjustments. The objective here is thus to expand analysis capabilities to enable modeling of the impact on aircraft noise due to advanced operational approach procedures, such as delayed deceleration approaches and thrust cutback scheduling on takeoff, for both current and future aircraft designs. Current industry standard noise models rely on flight test data interpolation and do not fully capture noise impacts from airframe configuration or advanced operational techniques. This is critical for noise assessment because airframe noise becomes a significant factor relative to the low thrust levels characteristic of advanced operational approaches. This method also limits the ability to assess new aircraft designs. Therefore, a new method combining aircraft sizing and performance tools with NASA's Aircraft NOise Prediction Program (ANOPP) has been developed to capture those noise impacts. ANOPP is used because of its capability of computing noise received at ground observers due to both engines and airframe of aircraft flying any flight procedure. Inputs into ANOPP are the aircraft geometry, the flight procedure, and the engine performance during the flight procedure. The Transport Aircraft System OPTimization (TASOPT) model is used to compute the engine performance inputs into ANOPP via first principles, physics-based methods. A separate tool was developed to compute the specifics of the flight procedure (max glide slope obtainable for a particular velocity and configuration, required thrust levels, etc.) based on drag polar supplied either by the Base of Aircraft Data (BADA 4) for current aircraft or by TASOPT for new aircraft. Benefits of this modeling framework include the flexibility in the aircraft and procedure analyzed and the ability to predict the noise of future aircraft configurations without relying on existing data. Both the noise impacts of a sample advanced operational flight procedure and in a future aircraft fleet have been assessed with this model. Next steps include further use of this model to evaluate the noise benefits or detriments of advanced operational approaches.

ACKNOWLEDGEMENTS

Table of Contents

1 Introduction

1.1 Motivation

Aircraft community noise has become a significant factor in the environmental assessment of aircraft and flight procedure designs. Advanced operational flight procedures with precise thrust, ground track, velocity, and configuration settings, along with continued changes or improvements in aircraft designs, present the possibility of continued noise reductions, although the extent of their improvements must be modeled before their improvements are deemed viable.

The primary tool currently used to assess aircraft community noise is the Aviation Environmental Design Tool (AEDT). AEDT utilizes the Noise-Power-Distance (NPD) based prediction method, which is an interpolation of flight test data in thrust and distance. This tool's estimations assume that airframe noise is insignificant compared to engine noise [1], which although may have been valid for earlier generation jet aircraft, is no longer valid for current generation aircraft whose engines have quieted significantly since the 1970's [2]. In present time, aerodynamic noise, which has been largely left constant over the years, is now one of the dominant aircraft noise sources, particularly in flight procedures where engine thrust (and therefore engine noise) is more moderate, such as in approaches or in certain advanced operational flight procedures. However these effects are not currently captured by AEDT's method. Additionally, the reliance on flight test data from existing aircraft for AEDT's noise computations makes the noise analysis of future aircraft using this method questionable. There is thus a gap in the ability to assess the noise impacts from both advanced operational procedures and future aircraft designs.

1.2 Thesis Overview

The research goal is to expand analysis capabilities to enable modeling of the noise impacts of advanced operational procedures for both current and future aircraft designs. This was accomplished by identifying the major sources of aircraft noise and how advanced operational procedures and future aircraft designs may serve to reduce those noise sources. Then, a robust noise analysis tool that takes into account engine and airframe noise and that is usable for both existing aircraft and future aircraft was identified and the various inputs required for usability of this tool and how their sources were obtained are presented. Noise results from the updated analysis capability were also validated against noise certification data as well as flight test data taken at Boston Logan Airport (BOS).

Use of the improved analysis method was then demonstrated on two sample cases to showcase its capability to model noise impacts of advanced operational procedures of current and future aircraft designs. The first is in the analysis of a sample single-event advanced operational flight procedure, the delayed deceleration approach (DDA), for which both airspeed and configuration changes play a significant role in the overall aircraft noise, an effect not capturable by the current standard analysis method and thus requires the improved noise analysis method. This example demonstrates the use of the model in assessing the noise benefits and drawbacks of an advanced operational flight procedure with complicated noise components, such as a DDA, where deployment of landing gear and high lift devices is delayed until later stages in the approach while the airspeed is maintained high. It is not immediately obvious whether the decrease in noise due to less engine power needed while the aircraft is kept clean outweighs the increase in noise due to increased airspeed for most of the flight. The improved noise analysis method was designed and shown to capture these impacts.

The second sample case is the analysis of the noise impact of a future aircraft fleet compared to a current baseline fleet, an analysis that requires the capability of modeling noise of future aircraft. In this example, an entire aircraft fleet at a sample airport was upgauged. Computing the noise impact of upgauging, or increasing the payload capacity and/or size of an aircraft, requires knowing the performance of aircraft that also do not have noise data associated with them, thus making the use of an NPD-based tool such as AEDT to analyze these noise impacts, which requires existing aircraft data, questionable. The combination of these two sample case studies thus showcases the full capabilities of the improved noise analysis method.

2 Background and Literature Review

2.1 *Definition of Aircraft Noise and its Metrics*

An aircraft in flight emits community noise, or noise that is heard by observers on the ground. Noise is merely unwanted sound that can be sensed as pressure waves over a wide range of amplitudes and frequencies. Noise intensity is measured in units of decibel (dB), which is a logarithmic ratio of the actual sound pressure level (SPL) to the threshold of hearing of 20 µPa.

While the audible frequency range for humans is 20 Hz to 20,000 Hz, humans are particularly responsive to and annoyed by frequencies in the 2 kHz to 4 kHz range. Thus, noise metrics are weighted at certain intensities and frequencies. Some common metrics for representing noise that are used in this thesis are as follows [3]:

- **LA_{max}**: The maximum A-weighted sound pressure level heard by an observer during an aircraft's entire flight. The A-weighting applied to this metric reduces the decibel values of sounds at low frequencies, as the human ear is less sensitive at low frequencies [3].

- **EPNL**: The Effective Perceived Noise Level is built from perceived noise levels, or measures of the human response to sound of constant intensity across the range of frequencies in the audible range. The perceived noise levels are further corrected at specific tones depending on their level above the local ambient sound level and their frequency. Finally for a given observer, the tone-corrected perceived noise levels received during an entire flight event that are within 10 dB from the maximum level received are integrated in time for a representation of annoyance due to the duration of the noise event. This final integrated number is the EPNL [3].

- **SEL**: The Sound Exposure Level at a particular observer, similar to EPNL, is an integration in time of noise levels heard from a flight event that are within 10 dB from the maximum sound level, as shown in *Figure 1*, and thus also is a measure of sound intensity and its duration. Rather than an integration of perceived noise levels however, this metric is an integration of A-weighted sound pressure levels [3].
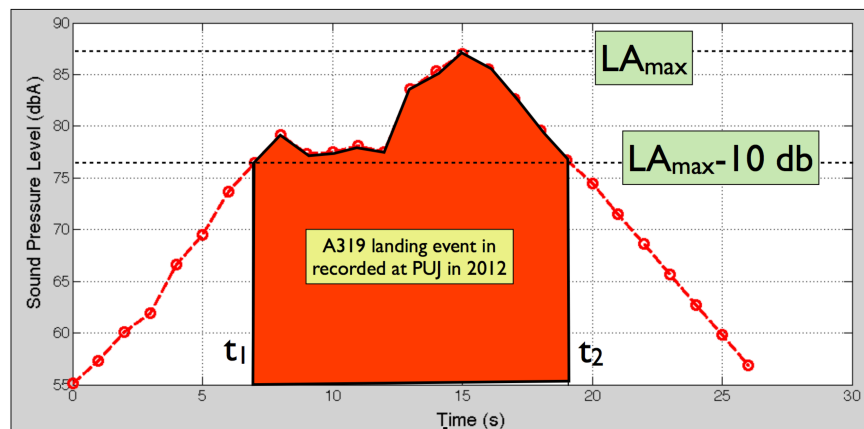
Figure 1: Sound Exposure Level Calculation, figure by A. Trani [4]

- **DNL**: The Day Night Average Sound Level is the average noise level over a 24-hour period and is computed as shown in *Equation 1* [4]. Ten to the power of the SEL

12

contours of all flights occurring during the day and ten to the power of the SEL contours occurring at nighttime between 10pm and 7am (summed with an additional 10 dB) are added together and normalized by the 86,400 seconds in a day. DNL is then equal to10 times the logarithm of this value.

$$DNL = 10 * \log\left[\frac{1}{86{,}400}\left(\sum_{day\,flights} 10^{\frac{SEL}{10}} + \sum_{night\,flights} 10^{\frac{SEL+10}{10}}\right)\right]$$

Equation 1: DNL, equation by A. Trani [4]

2.2   Primary Aircraft Noise Sources

The primary aircraft noise sources, as *Figure 2* highlights, are engine noise and airframe noise (More detailed descriptions of the aircraft noise sources are presented in section 3.1.1). Engine noise is composed primarily of [5]:

- Fan noise, or noise produced by turbulent air passing over fan blades, the interactions between fan rotor and stator vanes, and airflow passing over fan blade tips moving at supersonic speeds;
- Combustion noise, or noise produced from the combustion of hot gasses in the engine core;
- Jet noise, or noise produced from the fast airflow from the jet of the engine mixing with slower ambient air

Airframe noise is the remaining aircraft noise that would exist without the engines operating and is primarily due to airflow interacting with the aircraft's body. Airflow interacting with discontinuous surfaces such as the landing gear as well as lifting surfaces such as the wings, tails, flaps, and slats all contribute to airframe noise [5].
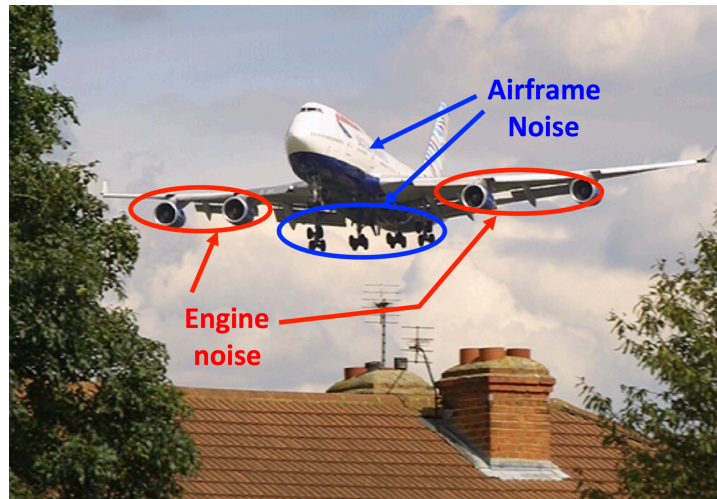
Figure 2: Primary Aircraft Noise Sources, Engine and Airframe

The distribution of engine and airframe noise dominance depends on the aircraft's flight procedure. An aircraft on departure is often in a state of high thrust and relatively clean

configuration once the landing gear is retracted. This leads to the engine being the dominant noise source compared to the airframe. However, the engines of an aircraft on approach are often in a relatively low thrust state while the aircraft is configured with high lift devices and landing gear extended in anticipation for landing. Thus, on approach, airframe noise tends to be as loud as or dominate to engine noise.

2.3   Aircraft Noise Improvements Since 1969 and Present Considerations

Increasing traffic of aircraft equipped with engines not originally designed for noise suppression in the late 1960's lead to great pressure for noise control around airports. This lead to the creation of Federal Aviation Rule Part 36 (FAR-36) in 1969, which set a limit on the maximum noise levels for certification of new aircraft [6]. With this rule in place, aircraft noise became a significant consideration in engine and aircraft design. One of the major design changes was transitioning from equipping aircraft with turbojets originally designed for military aircraft to equipping them with high-bypass ratio turbofans. This change, which has the benefit of improving propulsive efficiency on cruise [6], also leads to a reduction of jet noise by reducing the jet exit velocity (the reasons for this reduction in noise is further discussed in section 3.1.1). *Figure 3* shows a sample comparison of the 85 dB noise contour on departure of a 1960s Boeing 727 with a modern A320-200 equipped with modern high-bypass ratio CFM56 engines [2]. The contour has shrunk by nearly 9 times the original area, showing the significant noise reduction due to engine improvements.
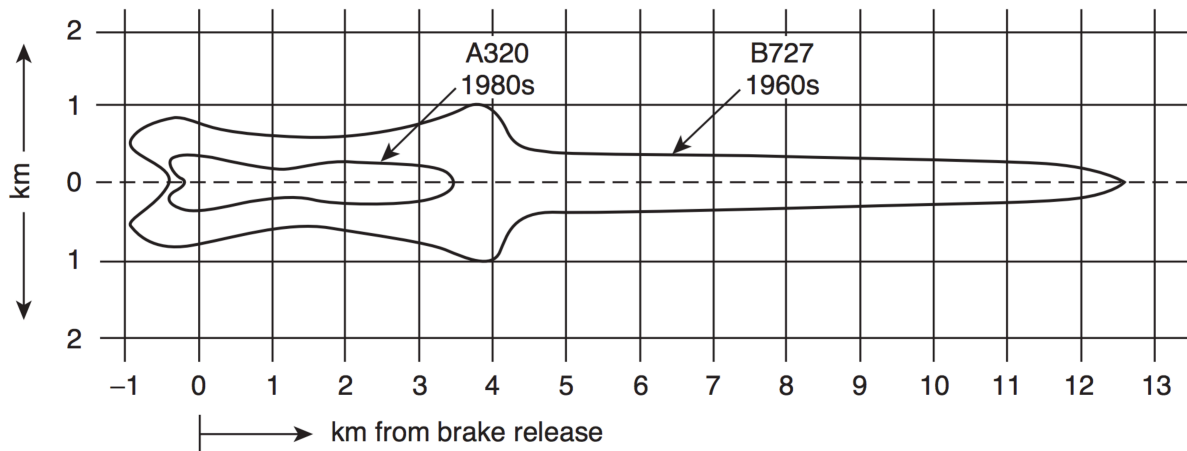
Figure 3: 85 dB Noise Contour of a 1960s Boeing 727 on Departure Compared to a Modern A320-200 [7]

Despite significant advancements in engine noise reductions, through examination of *Figure 4* it is apparent that airframe noise has become a much more significant factor in overall aircraft noise with each year. Aircraft noise in total continues to decrease as stricter noise standards are introduced. However as engines continue to be quieted, approach noise, where airframe noise is a dominating factor, is declining less rapidly than departure noise, where airframe noise is less significant. The importance of being able to model both engine and airframe noise to high fidelity is thus apparent as aircraft design continues to improve.

14
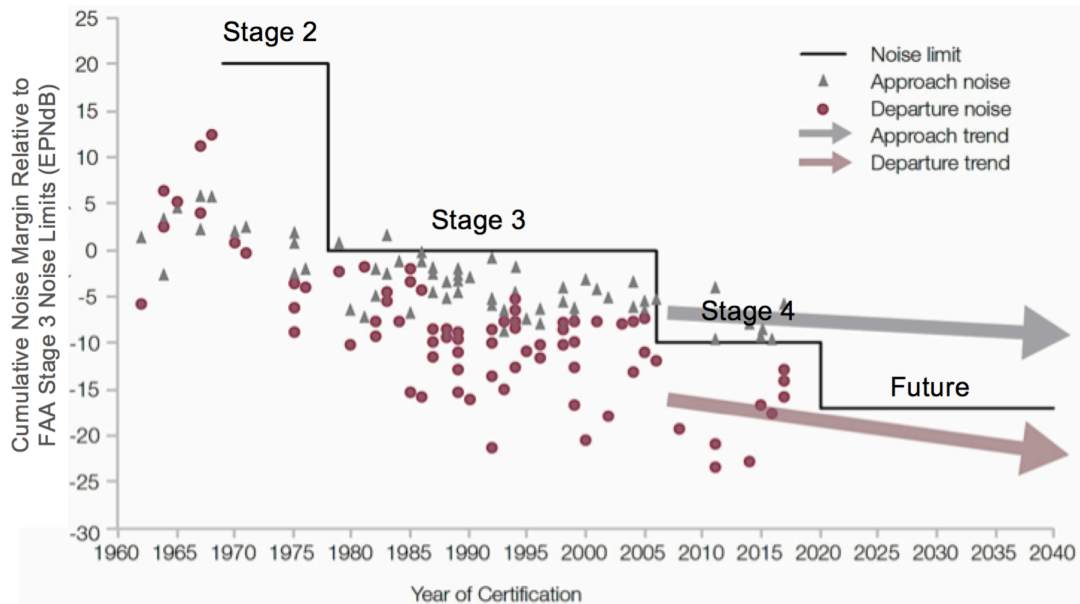
Figure 4: Historic and Predicted Aircraft Noise Trends by Year Show Less Decrease in Approach Noise Compared to Departure Noise [8]

Flight procedure adjustments and further advancements in aircraft design may be the path forward for continued noise improvements. Noise reduction techniques in the form of advanced operational flight procedures, where the aircraft's position, velocity, thrust, and configuration profile is precisely controlled, have also emerged and proven successful. Some examples include specific thrust cutback scheduling on departure at John Wayne Airport in Orange County, CA (KSNA) to reduce noise for sensitive areas around this airport [9] and optimized approach profiles where the aircraft glides near thrust idle to the runway at Seattle-Tacoma International Airport (KSEA) [10]. As noise standards become stricter and as commercial aircraft activity continues to increase with each year [11], it is essential for noise of both the current and future aircraft at both the aircraft design level and the flight procedure level to be properly evaluated.

2.4 AEDT's Noise Analysis Method and Its Limitations

The standard noise analysis tool used for evaluating noise around airports from new flight procedures is the FAA's model for the assessment of environmental impacts due to aviation, or the Aviation Environmental Design Tool (AEDT). AEDT uses the Noise-Power-Distance (NPD) method, where noise from flight test approach and departure data is treated as empirical data as functions of thrust level and configuration. The noise levels are then assumed to propagate to the observers on the ground assuming a standard atmosphere and consistent sound energy dissipation with distance [12]. An example set of NPD curves is shown in *Figure 5*.

Noise Power Distance (NPD) Curves
GE CF6-50 (Airbus A300)
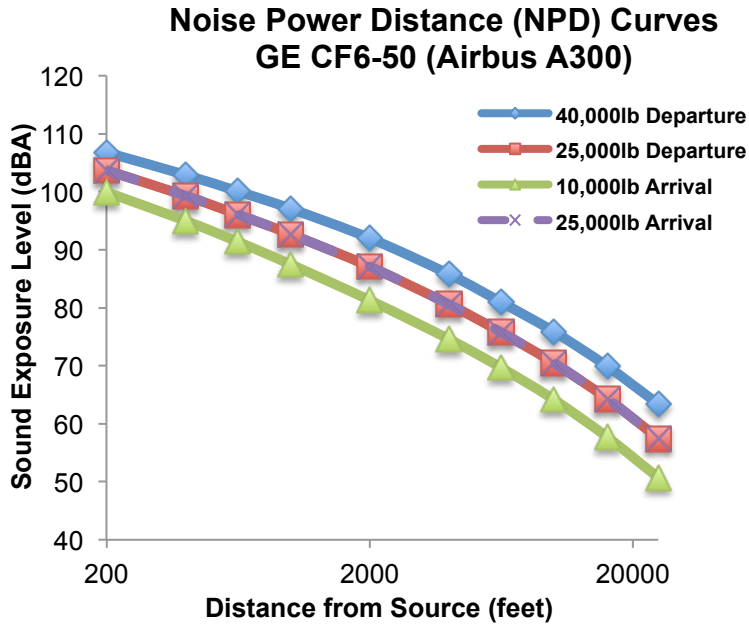
Figure 5: Sample NPD Curves for Airbus A300

Despite being the standard noise method for noise analysis around airports, AEDT is faced with two main limitations:

1. The flight data within the NPD curves that are used in AEDT's computations, in accordance with SAE Standard 1845a, are based on noise levels recorded with the aircraft flying at 160 kts true airspeed and set configurations. Thus, noise from an aircraft flying two scenarios, where in each the thrust is the same but the airspeeds and/or configuration are different, will be interpolated from the same NPD curve. Thus, noise changes due to changes in the aircraft's speed or variations in configuration are not captured with this method. For example, delayed deployment of landing gear and flaps could not be assessed using AEDT, as the NPD curves it uses were created assuming that the aircraft is in a set landing configuration throughout the procedure.

2. AEDT relies on test data from existing aircraft and therefore cannot be directly used to provide noise assessments of future aircraft.

3   Improved Noise Analysis Method

3.1   *Aircraft Performance and Optimization Tool to Component-Based Noise Analysis Tool*

The possibility of noise reduction via advanced operational procedures and future aircraft designs motivates the development for improvement in noise analysis methods beyond AEDT. One method of improvement is the use of noise models that capture the effects of various noise sources, shielding, and propagation, which need to be modeled with high fidelity to assess advanced operational procedures. They should also not be dependent on flight test data of each aircraft being modeled so as to be able to model future aircraft.

This section introduces an improved noise modeling method that is able to capture these impacts. The most integral portion of this framework is a higher-fidelity noise analysis tool, which computes noise from all noise source components individually, that is used to produce community noise grids for assessment of a hypothetical aircraft and flight procedure that created them. Such a tool requires an extensive set of inputs, which are outlined in *Figure 6*. Given an aircraft type or specification, an aircraft performance model (shown in pink) is used to generate aircraft performance, aircraft geometry, and engine performance parameters. Then, a flight mission specification and the aircraft's performance parameters are fed into a flight profile generator (shown in white) to generate the desired flight profile. The aircraft geometry, engine performance parameters, and the flight profile physically flyable by the aircraft are all fed into the noise model (shown in purple) for its final noise computations.
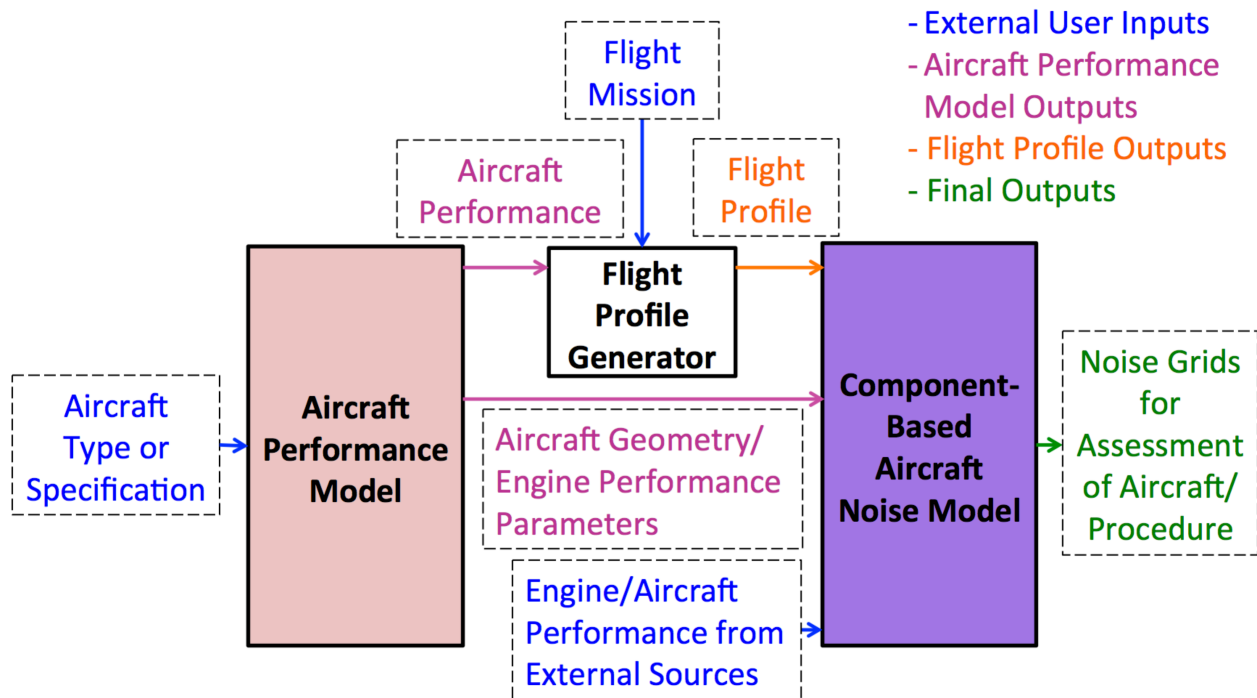
Figure 6: Outline of Improved Noise Analysis Modeling Framework

17

The component-based aircraft noise model and the theory behind its computation methods were first identified to determine the set of inputs required. Aircraft performance models that enable usability of this noise analysis tool for analyzing advanced operational flight procedures and new aircraft designs were then selected accordingly.

3.1.1 Component-Based Aircraft Noise Analysis Tool: the Aircraft NOise Prediction Program (ANOPP)

One such noise analysis tool with the functionality of analyzing noise at the component level is the Aircraft NOise Prediction Program (ANOPP) [13]. ANOPP is a NASA developed semi-empirical model that computes noise levels, such the contour shown in *Figure 7* (c), from the airframe and engine components (fan, core, and jet) at a user-defined 3-dimensional observer grid for an arbitrary flight procedure. It also accounts for propagation through a user-defined atmosphere and aircraft shielding effects for a higher-fidelity directivity analysis. ANOPP was developed as a series of modules (diagramed in *Figure 7* (b)) which each compute a particular noise component and its open documentation allows for interface with other tools. The modules used within ANOPP are semi-empirical, based on historical noise data, combined with physical noise models that are continuously updated with time. This makes ANOPP useful in providing noise predictions for a particular set of geometry and performance data without needing to know the specific aircraft in question, as well as providing predictions for an arbitrary flight procedure.

(a)

(b)
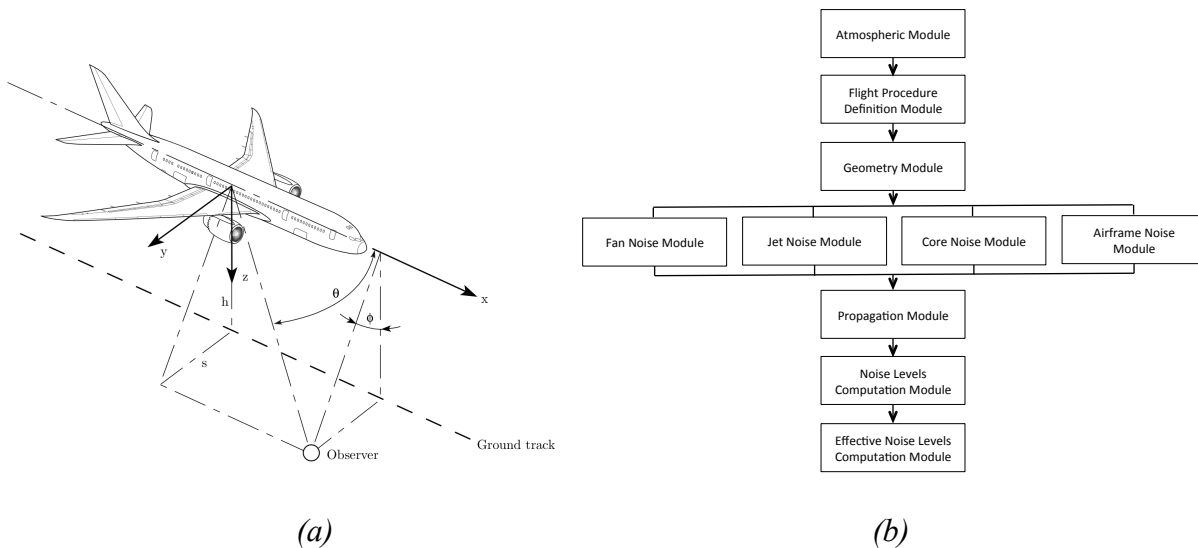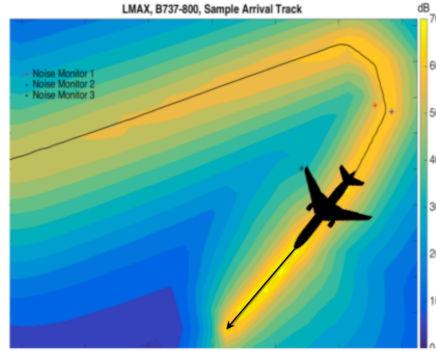
(c)

Figure 7: The Aircraft NOise Prediction Program [13] *Takes in an Aircraft and Flight Profile (a), Computes Source Noise for Each Component (b), & Sums the Source Noise Components to Produce a Final Noise Contour at All Observer Locations (c)*

ANOPP requires external models or data to supply all of the necessary aircraft and engine performance data needed to run the broadband noise (noise that occurs over a wide range of frequencies) and tonal noise (noise that occurs at specific frequencies) computations of all the components, described next.

The airframe noise components are computed in ANOPP based on the following phenomena:

- Airframe noise consists of many elements. The first element is the noise from the clean wings and tails due to convection of the turbulent boundary layer past the trailing edges. The sound level from this component is increased with boundary layer thickness that is a function of the area, the span, altitude, and the 5th power of the air speed.
- The second element due to leading edge slats that impact the wing boundary layer and thus increase the wing trailing edge noise as well as have trailing edge noise themselves.
- The third element is trailing edge flap noise that is produced by the lift fluctuations due to turbulence on the flap, which increases with increased flap extension and scales to the 6th power of velocity.
- Finally, the last element is landing gear noise, which is produced due to the deployed gear creating a break in an otherwise smooth surface. This element is dependent on the specific geometry of the gear's struts and wheels [13].

All of these components require the geometry of the specific components being analyzed, such as the area and span of the wings and tails and the strut length and wheel diameter of the landing gear.

The various engine noise components are computed in ANOPP based on the following phenomena:

- Fan noise consists of three main noise elements. The first is inlet and discharge broadband noise that are associated with unsteady flow passing the fan blades, creating turbulence. This noise element is related to the specific work across the fan, which is proportional to the temperature rise across the fan, and mechanical power, which is proportional to the mass flow rate through the fan. The temperature and mass flow rate through the fan are naturally inputs for this element of fan noise. The second element of fan noise is inlet and discharge discrete tone noise, which is

19

associated with lift fluctuations on the rotor blades and stator vanes. This component is dependent on the fan's rotational speed and on the number of rotor blades and stator vanes as well as their spacing. Making these components required inputs for the model. The last element of fan noise is inlet combination tone noise that is associated with shock waves that form at rotor tips at supersonic speeds. This element is thus also dependent on the fan's rotational speed [14].

- Core (or combustion noise) is attributed to the mass density and momentum fluctuation in the gas due to unsteady burning. It depends primarily on the air flow rates, temperature, and density through the combustor, making these performance characteristics necessary to compute noise of this component [13].

- Jet noise is attributed to turbulence created by a primary or core jet stream mixing with the slower secondary or bypass flow stream and the surrounding air. It also includes jet plug separation noise, a high frequency component associated with the primary stream. Jet noise scales with the difference of the velocities of the primary and secondary streams, the area, density, and temperature of the streams, and the area of the jet plug if it exists, making these performance characteristics necessary to compute the noise of this component [15].

Figure 8 shows these various engine performance inputs. Aside from the engine geometry inputs, these are needed at each time stamp in a flight profile to run ANOPP.
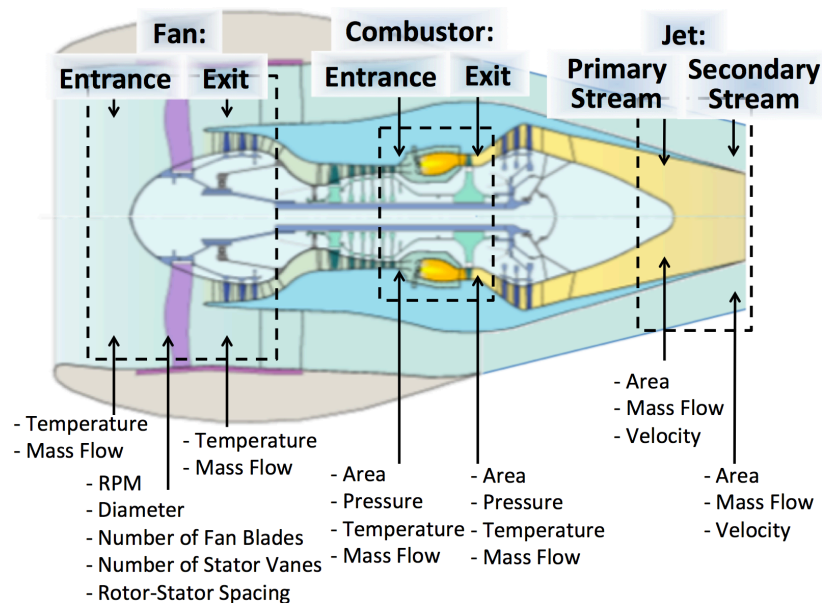
Figure 8: Diagram of Engine Inputs Needed as Functions of Speed, Altitude, and Thrust in ANOPP's Engine Component Noise Computations

A flight profile (position, velocity, thrust, and configuration vs. time) is thus also needed as an input. This is because at the noise source calculations, engine performance parameters vary with ambient flight velocity, thrust, and altitude, while airframe geometry parameters vary with aircraft high lift device and landing gear configuration. Also, to obtain the final noise received at any observer, the aircraft's position with respect to that observer versus time, as well as the conditions of the atmosphere, are needed.

Sound pressure levels at the aircraft sources are summed within ANOPP and propagated to the observer through user-specified atmospheric conditions. Sound intensity loss due to atmospheric attenuation is computed assuming losses due to thermal and viscous effects that are a function of temperature, pressure, and humidity as well as distance between the emitted noise at the source and the observer on the ground [13]. The user is able to compute additional engine installation shielding effects via two mechanisms. The first is a lateral attenuation correction according to SAE AIR 5662 for engine installation effects [16], diagramed in *Figure 9*. The second is a wing shielding model where attenuation is applied to sound waves from the engine that intersect with the aircraft's wings before radiating to the observer [13], diagramed in *Figure 10*, as a function of the sound wave frequency and distance from the edge of the wing surface.
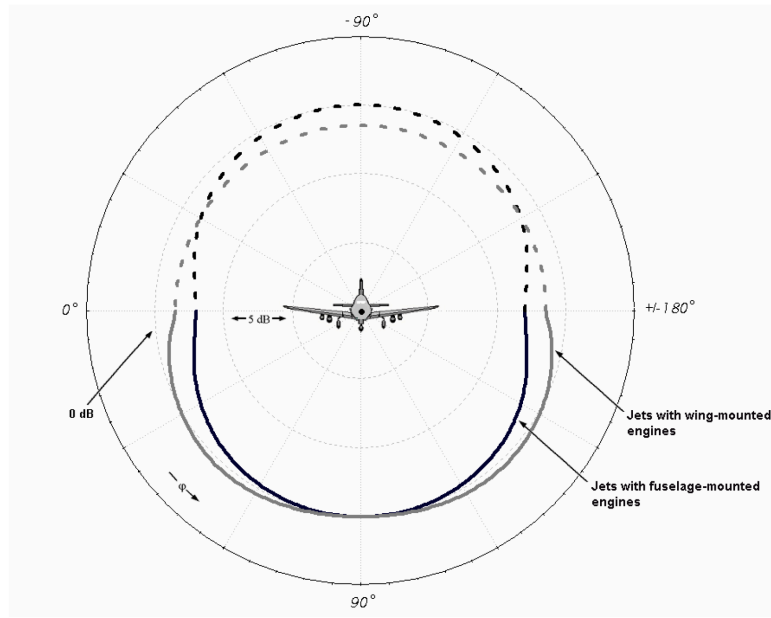
Figure 9: Engine Installation Corrections in ANOPP Based on the SAE AIR 5662 Method [16]
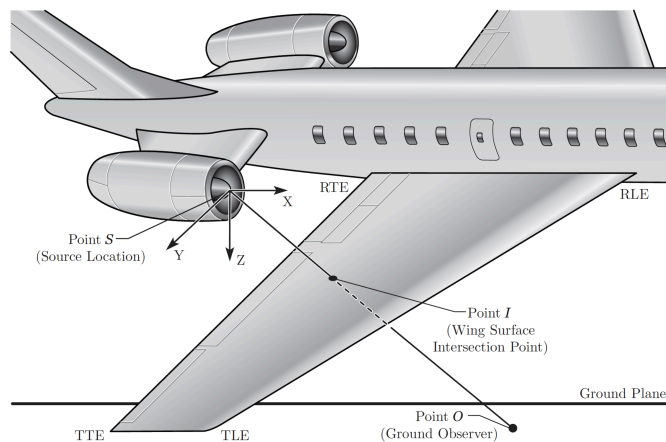
Figure 10: Coordinate System and Typical Propagating Sound Vector from Source to Observer for ANOPP's Wing Shielding Module [13]

Finally, A-weighted sound pressure levels and perceived noise levels are computed at each observer location during the entire flight profile. The maximum A-weighted sound pressure level

is reported as LA_{max} for the flight profile. The A-weighted sound pressure levels and perceived noise levels are also integrated in time to produce SEL and EPNL at each observer.

In summary, ANOPP requires a thorough list of engine performance parameters, engine geometry, airframe geometry, and a flight profile to run. Additional models thus must be identified to supply all of these inputs.

3.1.2 Aircraft Performance Model: Transport Aircraft System OPTimization (TASOPT)
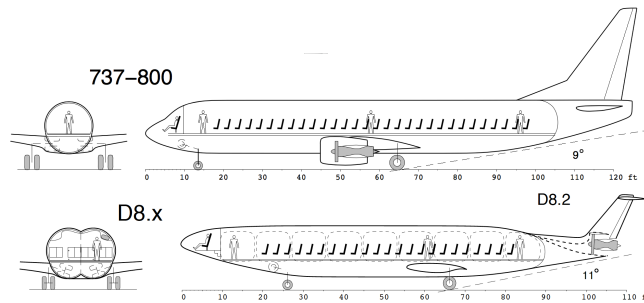
Figure 11: The Transport Aircraft System OPTimization Program [17]

The primary model chosen to supply the aircraft performance parameters needed for ANOPP is the Transport Aircraft System OPTimization (TASOPT) program [17]. TASOPT was developed by Professor Mark Drela at MIT as a tool to jointly optimize the airframe, engine, and flight trajectory of a "tube and wing" transport aircraft using first-principles physics based methods, rather than relying on traditional empirical drag and weight prediction methods. Both current and future aircraft, such as those in *Figure 11*, can thus be modeled and analyzed in this program--a feature that is needed for the analysis of the scope of aircraft in this modeling method.

TASOPT requires a set of operating and mission requirements, aircraft sizing and performance parameters, and engine sizing and performance parameters to size an aircraft. These can be matched to an existing aircraft type's specifications when modeling an existing aircraft or be modified for a future aircraft concept. The user's required inputs, and how they are used in TASOPT's initial sizing computations, are as follows:

1. The user specifies the aircraft's mission requirements. These include the aircraft's weight per passenger, load limits, maximum range, number of passengers, start of cruise altitude, and cruise Mach number. The weight per passenger is assumed to follow standard average passenger weights listed in Advisory Circular 120-27E [18] while the aircraft load limits follow the minimum required structural load limits described in 14 CFR 25.333 and 25.337 [19]. The remaining parameters are readily available for existing aircraft types in *Jane's All the World's Aircraft* [20]. This information thus becomes the basis for subsequent calculations.

2. The airframe structure is then modeled as simplified geometric shapes and is sized assuming critical loading cases for each component. The user inputs the geometry of the fuselage including the fuselage diameter, fuselage length, height of the fuselage floorboard, and location of aircraft sub-components along the length of the fuselage such as the auxiliary power unit location and the landing gear location. The fuselage skin, stringers, and floor are sized assuming the aircraft is a pressure vessel to meet various loading scenarios, while the weights of secondary components such as windows, seats,

etc. are estimated using historical weight fractions which are proportional to the number of passengers. The user also defines parameters regarding the shape of the wings and tails, such as the sweep, aspect ratio, taper ratio, thickness-to-chord ratio, and tail volumes, as well as historical weight fractions for secondary wing components such as the slats, flaps, etc. These parameters are then assigned to the wings and tails, which are then sized to survive critical bending loads at the maximum allowable load limit cases. The internal size of the wing also gives the maximum fuel volume. The geometry parameters needed for the fuselage, wing, and tail sizing are obtained from detailed aircraft CAD drawings found within airport planning guides for existing aircraft, while the weight fractions are typically held constant at historical values.

3. Aerodynamic performance is next modeled assuming that lifting forces balance weight while drag balances thrust, which thrust computed as a power balance derived by Drela [17]. A parameterized transonic airfoil family spanning a range of thicknesses is used to obtain airfoil lift and drag performance that is applied to the 3-dimensional wing. The fuselage drag is obtained from viscous/inviscid CFD based on the user-supplied fuselage geometry. Nacelle drag is obtained assuming it is a power dissipation based on the nacelle's exterior velocity distribution. Finally, overall drag is predicted using a Trefftz-Plane analysis.

4. TASOPT next uses a detailed component-based turbofan model using the layout shown in *Figure 12* to size the engine. The calculations are based on Kerrebrock methods [21] to obtain the engine areas, temperatures, pressures, and mass flow rates at the various stations within a turbofan. The user must supply the engine's maximum turbine inlet temperature T_{t4}, the bypass ratio, and pressure ratios and efficiencies of the various engine components for this method. The engines are then sized for cruise and after which are examined in an off-design mode to obtain engine parameters for any other phase of the aircraft's trajectory.
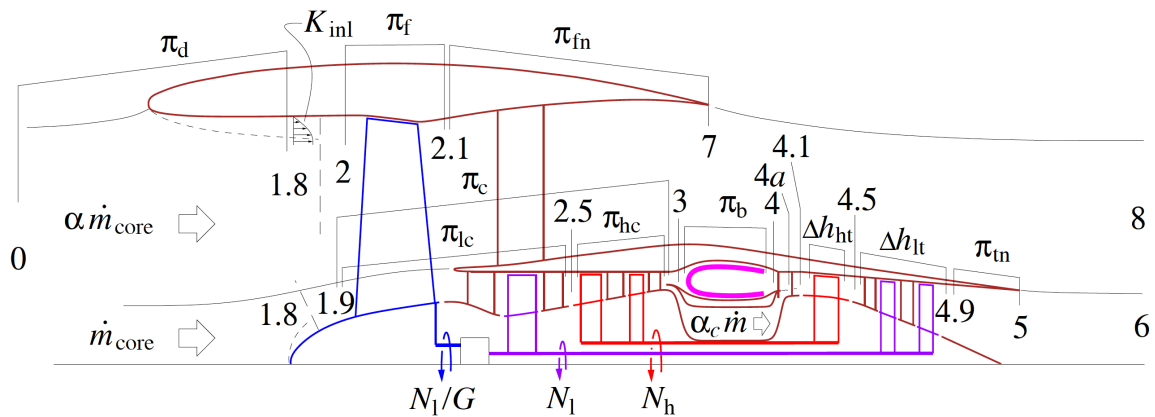
Figure 12: Turbofan Engine Layout Used in TASOPT's Engine Calculations [17]

Many engine technology levels that the user is required to input for this method, such as overall pressure ratio and fan pressure ratio can be obtained from resources such as *Jane's Aero-Engines* [22] for a specific engine. Some properties such as maximum T_{t4} can be approximated based on historical engine charts of T_{t4} versus overall pressure ratio, bypass ratio, and specific fuel consumption such as that in *Figure 13*. Some remaining engine technology levels that aren't obtainable from publically available resources, primarily

engine component efficiencies, are held at constant values across various aircraft types that are based on Drela's consultations with engine manufactures.
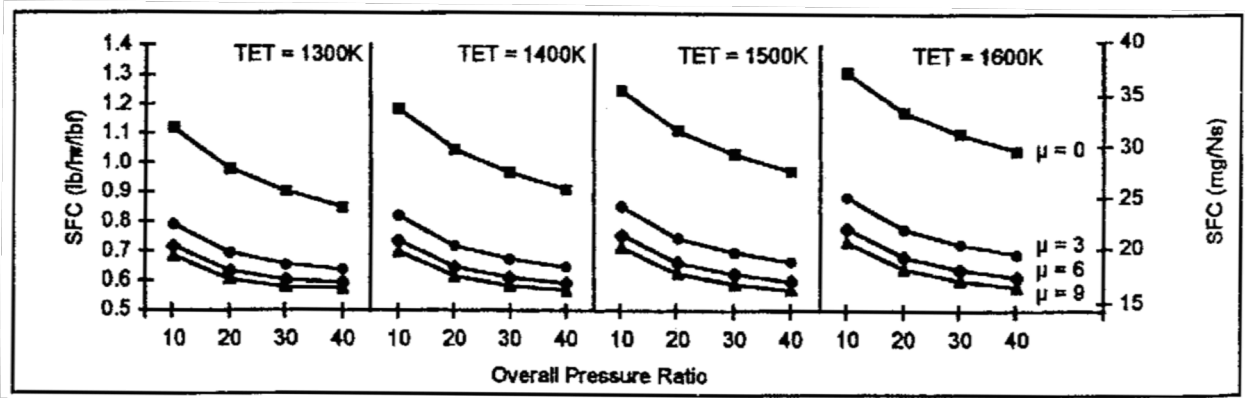
Figure 13: Turbofan Specific Fuel Consumption Variation with Bypass Ratio (μ), Turbine Entry Temperature (TET), and Overall Pressure Ratio [22]

Given all of the user defined information described above, TASOPT carries out the remainder of the aircraft sizing as follows:

5. The various weights and locations of the aircraft and the overall aircraft pitching moment from the aerodynamic analysis are then used to enforce pitch stability, which then sets the locations of the aircraft tails.

6. The aircraft trajectory is computed on a segment-by-segment basis assuming a cruise-climb during the aircraft's cruise at a fixed cruise Mach number, cruise lift coefficient, and cruise T_{t4}. Higher T_{t4} values inputted by the user are used to set the climb profile while the decent is set by a constant descent angle resulting in T_{t4} on descent becoming an output. Balance field length is also checked in a takeoff performance model.

7. A variation in the initial fuel weight is repeated until the range from this trajectory generation equals the initial design range specified by the user. An aircraft that meets the mission requirements given the aircraft shape (its fuselage geometry and wing shape) and the technology level (weights of various secondary components, engine pressure ratios, etc) is thus completely sized.

The critical outputs from TASOPT for use within the improved noise analysis method framework are the aircraft performance, aircraft and engine geometry, and engine performance parameters first introduced in *Figure 6*. The details of these outputs, which outputs are used, and how those outputs are used within the improved noise analysis method framework is as follows:

- The used aircraft performance outputs are the aircraft's maximum takeoff weight, takeoff roll length, maximum takeoff and climb thrust, and V2. These aircraft performance outputs are fed to the flight profile generator described in section 3.1.3. The aircraft weight is also used to size the number of and the diameter of the wheels of the nose and main landing gear of the aircraft for use within ANOPP's airframe noise computations. This implementation is described in Appendix A.2.

- The used aircraft geometry outputs are the aircraft's wing and tail areas and spans. These feed directly into ANOPP's airframe noise computations. The used engine geometry outputs are the area and diameter of the engine fan. Flap area and span, as well as landing gear strut length, are not direct outputs from TASOPT. Instead, TASOPT's outputted wing area and span, as well as engine diameter, are also used to

24

infer the necessary geometry of the flaps and the landing gear strut length for use within ANOPP's airframe noise computations. This implementation is described in Appendix A.2 and Appendix A.3. Additionally, TASOPT provides the geometry of the wing with respect to the engine position that is needed for ANOPP's wing shielding computations.

- The used engine performance outputs are tables of pressure, temperature, areas, and velocity, such as that shown in *Table 1*, as well as the core mass flow rate, bypass ratio and fan rotational N1 speed that is provided at each ambient Mach number, engine thrust, and aircraft altitude. These all feed into ANOPP's engine noise computations.

```
B2: alt.   =   8375. ft
B2: Mach   =  0.4713
B2: BPR    =  5.0970
B2: N1     =  1.0635
B2: Feng   =  62.051      kN
B2: mcore  =  50.867      kg/s

B2:  loc      Tt       pt       cpt       R      cpt/(cpt-R)
              K        kPa      J/kg K   J/kg K
      0      283.6     86.24    1008.7    288.3    1.4002
      2      283.6     85.81    1008.7    288.3    1.4002
      21     331.8    141.46    1011.1    288.7    1.3989
      7      331.8    138.63    1011.1    288.3    1.3989

      0      283.6     86.24    1008.7    288.3    1.4002
      18     283.6     85.81    1008.7    288.7    1.4002
      19     283.6     85.81    1008.7    288.7    1.4002
      25     378.9    214.14    1014.9    288.7    1.3968
      3      815.1   2565.67    1105.6    288.3    1.3527
      4     1509.0   2411.73    1265.7    288.8    1.2956
      41    1423.0   2256.59    1248.5    288.7    1.3008
      45    1052.3    547.08    1189.6    288.7    1.3205
      49     759.9    128.63    1122.2    288.7    1.3464
      5      759.9    127.99    1122.2    288.7    1.3464

B2:  loc      T        p        M        u        A        Fsp      eta_p
              K        kPa              m/s      m^2
      0      271.6     74.12   0.4713   155.66   2.0943   0.6058
      2      264.6     67.31   0.5993   195.87   1.7944

      25     353.5    167.76   0.6013   226.98   0.1361

      5      659.2     74.12   0.9300   472.74   0.2810
      6      659.2     74.12   0.9300   472.74   0.2810   0.1615   0.4954

      7      277.5     74.12   0.9896   331.18   0.8448
      8      277.5     74.12   0.9896   331.18   0.8448   0.4443   0.6395
```

Table 1: Example Table of TASOPT's Engine Performance Outputs at Each Station of a Sample Engine at One Specific Mach Number, Thrust, and Altitude Operating Point

While TASOPT's aircraft and geometry performance outputs for an existing aircraft can be found in sources such as *Jane's All the World's Aircraft* [20], the engine performance outputs are not readily available from manufacturer websites. Thus TASOPT is useful within the improved noise analysis method framework not only for providing aircraft performance, aircraft and engine geometry, and engine performance parameters of future aircraft by physics-based calculations, but also by providing the engine performance parameters in the detail that is required by ANOPP for existing aircraft types.

3.1.3 Flight Profile Generator

The final piece needed to complete the improved noise analysis method is an additional model for simulating the position, velocity, and thrust of an aircraft based on its performance capabilities and that also provides the user with the ability to model very specific flight procedures. A model based on basic force-balance and kinematics was thus created to fulfill this role. The primary free body diagram for any given time in flight is shown in *Figure 14*.
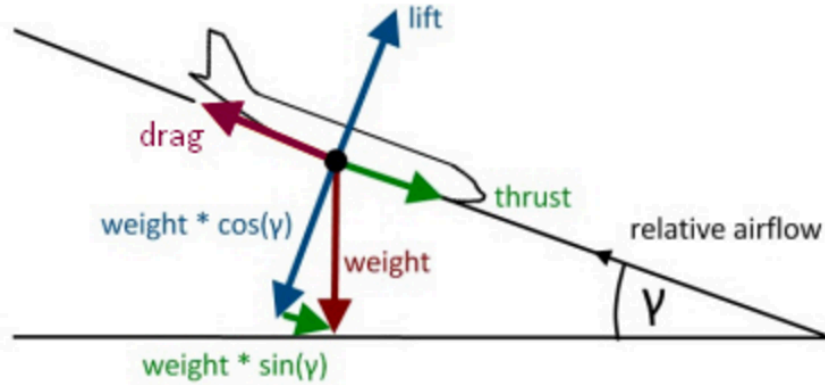
Figure 14: In-Flight Free-Body Diagram Used for the Flight Profile Generator

The acceleration of the aircraft along the direction of flight is thus given by the sum of the forces in the direction of flight divided by the mass of the aircraft shown in *Equation 2*:

$$a = \frac{\sum Forces}{m} = \frac{Thrust + Weight * \sin(\gamma) - Drag}{Weight / g}$$

Equation 2: Acceleration in the Direction of Flight

With the acceleration of the aircraft known, the distance traveled along the aircraft's flight path, s_{end} - s_{start}, or the change in altitude, z_{end} - z_{start}, given a change in velocity V_{end} - V_{start} can be determined from kinematics, shown in *Equation 3*:

$$\frac{(V_{end})^2 - (V_{start})^2}{2a} = s_{end} - s_{start} = \frac{(z_{end} - z_{start})}{\sin(\gamma)}$$

Equation 3: Change in Position with Change in Velocity

A takeoff or landing roll is treated slightly differently given that the aircraft also overcomes friction from being on the ground. The free-body diagrams assumed in takeoff and landing are shown in *Figure 15*. The sum of the forces in *Equation 2* is adjusted accordingly.
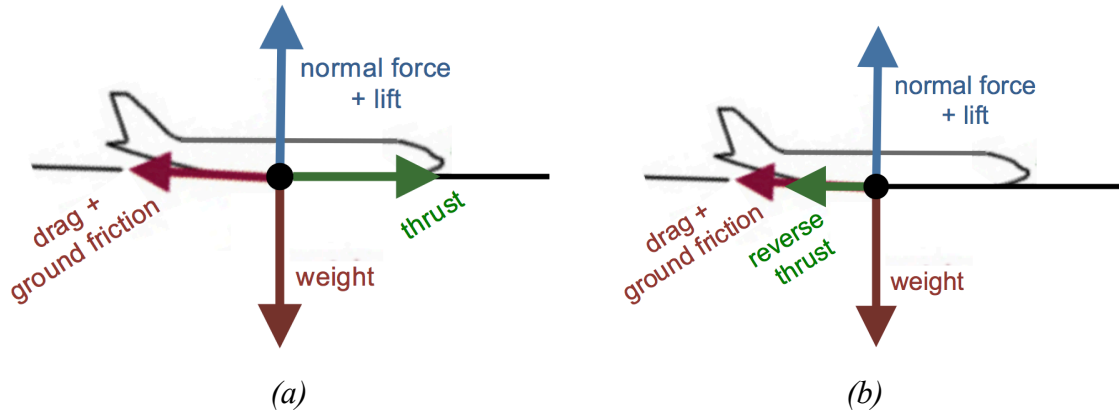
Figure 15: Takeoff-Roll (a) & Landing-Roll (b) Free-Body Diagrams Used by the Flight Profile Generator

Given the aircraft's weight and drag coefficients, the user is able to build up the flight profile segment-by-segment using a combination of *Equation 2* through *Equation 3* at each segment. To initiate the flight profile generation, the user first specifies an initial condition in the flight procedure that is known. For a departure, this initial condition is typically the start of the takeoff roll, where the aircraft's starting position and zero velocity are known. For an approach, this initial condition is typically the location of aircraft touchdown on the runway, where the aircraft's touchdown position and velocity are known. With the initial conditions known, user then specifies the position end conditions and thrust requirements of the flight segment. For position, these can include: the ending velocity, the ending flight path distance, the ending altitude, or the glide path angle. For thrust, these can include required thrust to carry out a particular acceleration in a given distance or a specified thrust value, such as idle thrust or max takeoff thrust. The profile generator then computes the remaining conditions about the flight segment not yet specified, as listed in *Table 2*. Finally, the ending conditions of one segment become the initial conditions of the next segment and the process continues for all flight procedure segments.

Segment Type Description	Segment Required Parameters	Computed Parameters
Takeoff/Landing roll at a user defined thrust or reverse thrust	Ending Velocity, Thrust	Ending s Position, Ending z Position
Takeoff/Landing roll at required thrust or reverse thrust for a user defined roll length	Ending Velocity, Takeoff Roll	Ending z Position, Thrust
Travel to s at required thrust to a user defined ending velocity	Ending Velocity, Ending s Position, Flight Path Angle	Ending z Position, Thrust
Travel to s at defined thrust to a user defined ending velocity	Ending Velocity, Ending s Position, Thrust	Ending z Position, Flight Path Angle
Travel to z at required thrust to a user defined ending velocity	Ending Velocity, Ending z Position, Flight Path Angle	Ending s Position, Thrust
Travel to z at defined thrust to a user defined ending velocity	Ending Velocity, Ending z Position, Thrust	Ending s Position, Flight Path Angle
Accelerate at defined thrust to a user defined ending velocity	Ending Velocity, Thrust, Flight Path Angle	Endings Position, Ending z Position

Table 2: Flight Profile Generator Inputs and Outputs for Each Segment Type

This methodology is used to then design new flight procedures given a select number of segments, such as that shown in *Figure 16*, or to compute the thrust expected given flight recorder velocity and position data, such as that shown in *Figure 17*. To compute the thrust of the latter, each segment is defined with the known velocity at subsequent data points. Then given the known distance between subsequent points and an assumption for the aircraft's configuration to solve for the drag, the acceleration and finally thrust can then be computed. A specific example methodology for assuming the aircraft's configuration when using the profile generator to determine thrust from flight test data is discussed further in section 4.2.
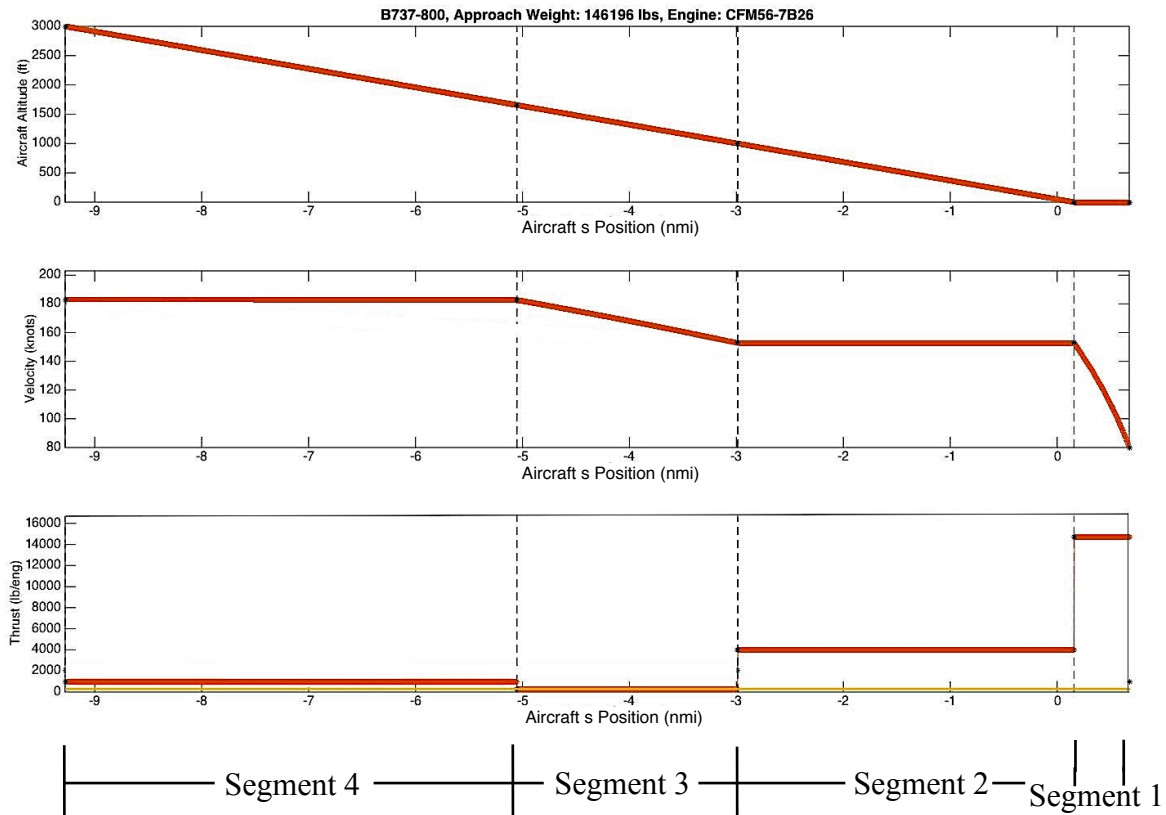
Figure 16: Example of Sample Segment-by-Segment User Built Flight Procedure
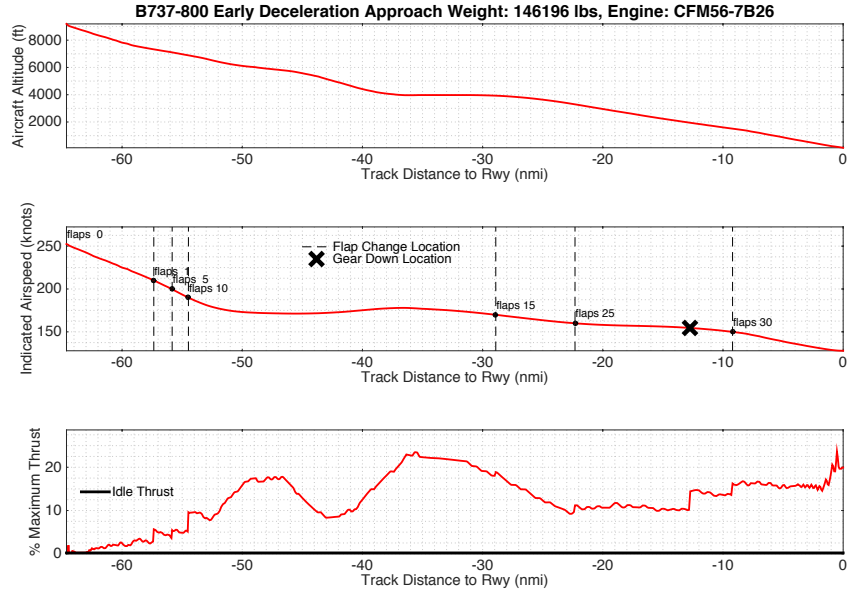
Figure 17: Altitude and Velocity from B738 Flight Test Data and Thrust as Computed in the Profile Generator

With the altitude versus along track distance computed, the flight profile is finally fitted to the lateral flight track desired for this procedure. The flight track is often specified by set of latitudinal and longitudinal waypoints converted into <x,y> pairs that the aircraft must fly through. Because the along track distance is defined in *Equation 4*. Thus at any point along the flight trajectory, only a specific change in lateral position x and y can satisfy *Equation 4* for a given change in along track distance s and altitude z. This computation is computed for the entire altitude versus along track distance profile to fit the flight profile along a flight track such as that shown in *Figure 18*.

$$\Delta s = \sqrt{\Delta x^2 + \Delta y^2 + \Delta z^2}$$

Equation 4: Change in Along Track Distance vs. Lateral Position and Altitude
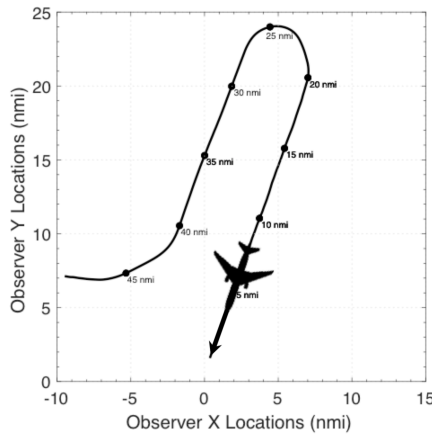
Figure 18: Sample 50 nmi Approach Flight Profile Fitted to <x,y> Track as Computed in the Profile Generator

29

3.1.4   Finalized Improved Noise Modeling Framework

The final improved noise analysis framework with all tools combined is diagramed in *Figure 19*, where text describing user inputs are represented in blue, tools are represented in black, TASOPT generated outputs are in magenta, the flight profile is in orange, and final noise outputs are in green.
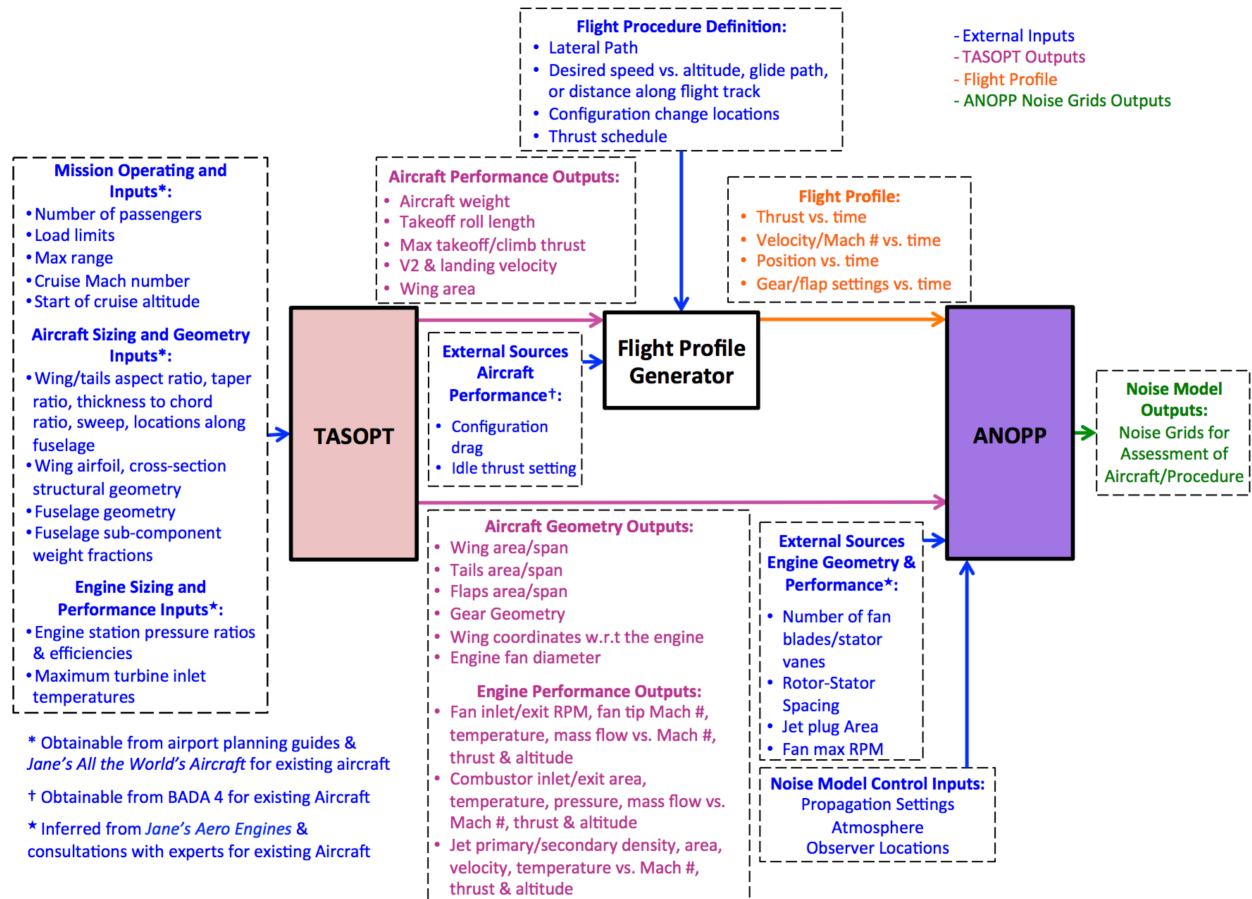
Figure 19: Final Improved Noise Analysis Modeling Framework

To analyze the performance and noise of a particular aircraft and flight procedure, an aircraft type or specification is first fed into TASOPT in three sets. The first set is operating and mission parameters, or the number of passengers, load limits, cruise Mach number, max range, and start of cruise altitude. The second set is the aircraft sizing and geometry parameters, or the wing and tail taper, thickness to chord, and aspect ratios, sweeps, and locations along the fuselage, the wing airfoil and cross-section geometry, the fuselage geometry, and weight fractions of fuselage subcomponents. These two sets of data can be obtained from airport planning guides and *Jane's All the World's Aircraft* [20] for existing aircraft or uniquely set by the user when modeling a future aircraft. The third set of data is engine sizing and performance inputs, or the engine station pressure ratios and efficiencies, as well as the maximum turbine inlet temperature at takeoff and cruise. These inputs can be estimated for both existing and future aircraft from engine performance tables in *Jane's Aero-Engines* [22] such as that back in *Figure 13*. However some engine technology levels that aren't obtainable from these publically available resources, primarily engine component efficiencies, are held at constant values across various aircraft types that are based on Drela's consultations with engine manufactures.

TASOPT then outputs aircraft and engine performance and geometry parameters. The aircraft performance outputs include the aircraft weight, takeoff roll length, maximum takeoff and climb thrust, and V2 and landing velocity. These, along with the wing area, all become inputs to the flight profile generator. TASOPT does not provide drag polars as a function of configuration at the time of this thesis, therefore additional configuration drag polars must also be supplied to the profile generator from external sources. One source of drag polars for existing aircraft is Eurocontrol's Base of Aircraft Data (BADA 4) [23] (an example usage of which is in section 6.3.2), a database of aircraft performance parameters obtained from aircraft manufactures. BADA 4 also serves as a source of data for idle thrust settings as desired. While BADA 4 is one option to supply drag polars, the user can supply drag polars from other sources as desired. Given external flight profile data or the user's definition of the flight procedure, including the lateral path, speed and altitude or position targets, and configuration, the flight profile generator then builds the full position, velocity (and ambient Mach number), thrust, and configuration profile per time of the aircraft that is physically realizable based on TASOPT's aircraft performance outputs. This feeds directly into ANOPP, as detailed in Appendix A.1.

TASOPT also outputs aircraft geometry parameters, namely the wing and tail areas and the engine diameter. Flap area and span are inferred from the wing area and span and the landing gear geometry is sized based on the aircraft's maximum weight and engine diameter, as described in Appendix A.2. Along with geometry, TASOPT also outputs engine performance parameters characteristic to the fan, combustor, and jet at various Mach number, thrust, and altitude settings. These are inputted into ANOPP as detailed in Appendix A.3.

In addition to the TASOPT outputs, additional engine geometry and performance data not available from TASOPT is gathered as needed. This data includes the number of fan blades, number of stator vanes, and maximum RPM of the engine, which TASOPT's Kerrebrock methods do not compute. This additional needed engine information is typically found in references such as *Jane's Aero-Engines* [22] for existing aircraft. These are inputted into ANOPP as detailed in Appendix A.4.

Finally, the required aircraft and engine performance and geometry parameters, the flight profile, and some additional noise model control inputs such as the user defined atmosphere, propagation settings, and the three dimensional grid of observer locations are all fed into the ANOPP noise model as detailed in Appendix A.5. ANOPP outputs noise of the components the user wishes to analyze (these can be any specific engine component, the entire engine, the airframe only, or all noise components) for this single procedure in the form of LA_{max}, SEL, or EPNL. Noise at a single observer on the ground can be computed and compared to noise monitor data or an entire grid can be superimposed with other grids to be combined into other metrics such as DNL to observe noise impacts of an entire aircraft fleet.

This modeling framework improves upon the noise modeling limitations of the NPD method in the following ways:

- Provides a noise assessment of both airframe noise and engine noise on a component basis through ANOPP's modular analysis framework at a variety of speed and configuration settings;
- Provides the ability to assess a wide variety of flight procedures through the flexibility in building the flight profile in the flight profile generator;
- Provides the ability to assess the noise of both current and future aircraft using TASOPT's flexible aircraft sizing

31

4   Validation of the Improved Noise Analysis Method

4.1   Validation of Method with Noise Certification Data

Noise results from the improved noise analysis method were compared to existing noise certification data as initial validation of the method. The noise of civil aircraft has been recorded for certification at three specific observer locations with the aircraft flying three specific flight procedures. The details of the flight procedures and the observer locations are given in 14 CFR Part 36 [24]. In summary, each aircraft flies the procedures and effective perceived noise levels (EPNL) are recorded at the observer locations summarized in *Table 3* and *Figure 20*. They include a flyover profile and observer directly under the departure flight path (flyover reference), an approach profile and observer directly under the approach path (approach reference), and a lateral profile and observer offset from the runway at the loudest point of the departure (lateral reference).

Procedure	Speed (kts IAS)	Configuration	Thrust
Flyover	V2+10kt to V2+20kt	2nd Setting from clean	Max TO to 300 m altitude, then reduced to maintain 4% climb gradient
Approach	Vref+10kt	Full Flaps + gear	As required to maintain 3° glideslope
Lateral	V2+10kt to V2+20kt	2nd Setting from clean	Max TO

Table 3: Description of Noise Certification Flight Profiles
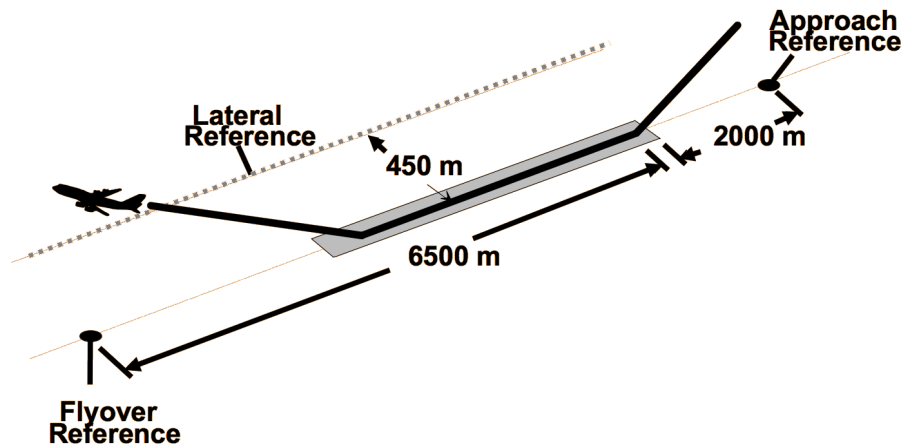
Figure 20: Noise Certification Observer Locations

Six aircraft were modeled using the improved noise analysis method and the results are presented below. An agreement within -2.24 to 3.71 dB between the ANOPP noise results and the certification data was found for each of these six aircraft and the three observer locations,

with many of the measurements agreeing within 1 dB of the recorded value. Discussions with noise experts indicate that measured noise data can have a scatter of 15 dB [25]. In addition, aircraft flying noise certification test profiles do not always fly the procedures exactly as defined in 14 CFR Part 36. Thus these results are considered good agreement and thus are sufficient to warrant the use of the model.

(a)

(b)

(c)

(d)
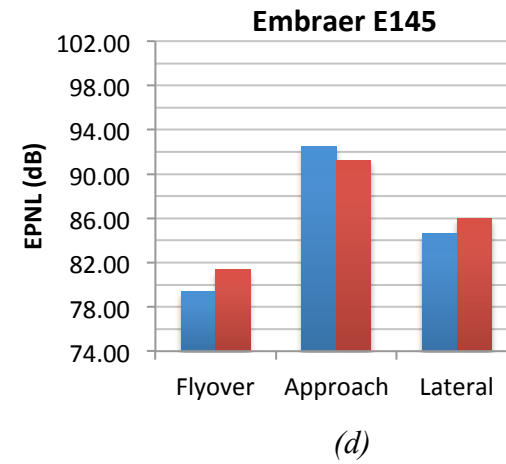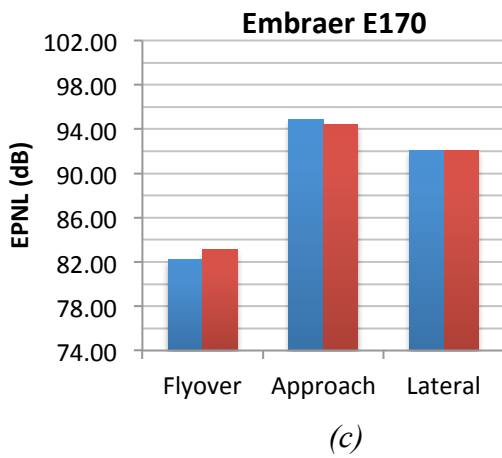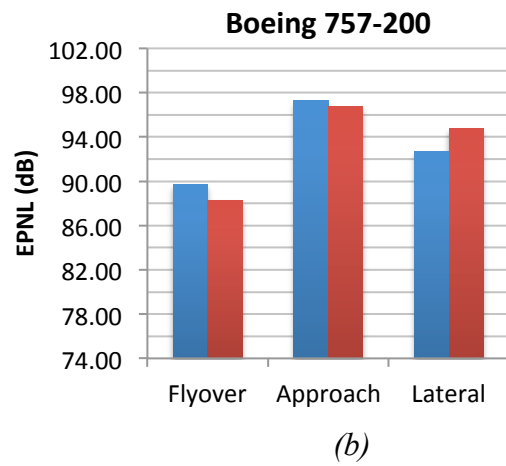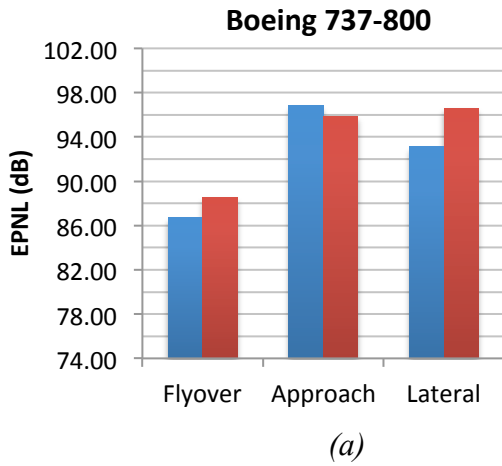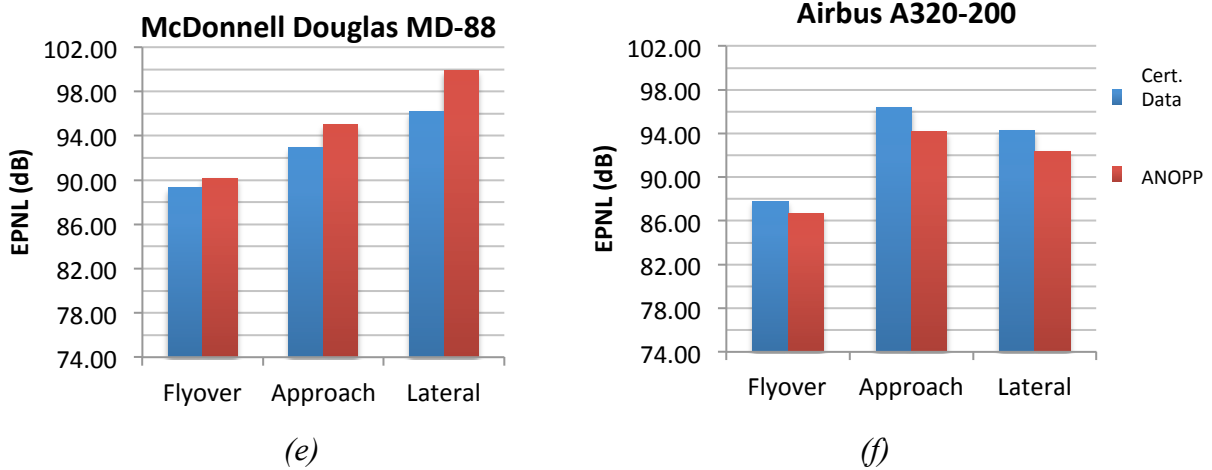
*Figure 21: EPNL (dB) of B738 (a), B752 (b), E170 (c), E145 (d), MD88 (e), & A320 (f)
Computed with ANOPP and Reported in FAA Noise Certification Data* [26]

4.2 Validation of Method with Data from Existing Boston Logan Airport Operations

A validation of the improved noise analysis method's ability to assess noise from flight track radar data of existing flights was also done via a noise measurement campaign performed by MIT Lincoln Laboratory [25]. Three Brüel & Kjær Noise Sentinel monitor systems were placed at the noise monitor (NM) locations diagramed in *Figure 22* to record noise data of flights on approach to Boston Logan Airport (BOS) runways 22L/22R from November 13, 2015 to January 25, 2016. Flight track radar data was also collected for each flight and correlated for each noise event. This data was used to obtain groundspeed of the aircraft and was converted into true airspeed using a wind vector determined from the North American Regional Reanalysis (NARR) data interpolated in space and time to the aircraft position, and from there was converted to indicated airspeed (IAS) using the appropriate atmospheric corrections. LA_{max} and SEL were then computed at all noise monitors that the aircraft flew within 0.5 nmi in lateral distance of.
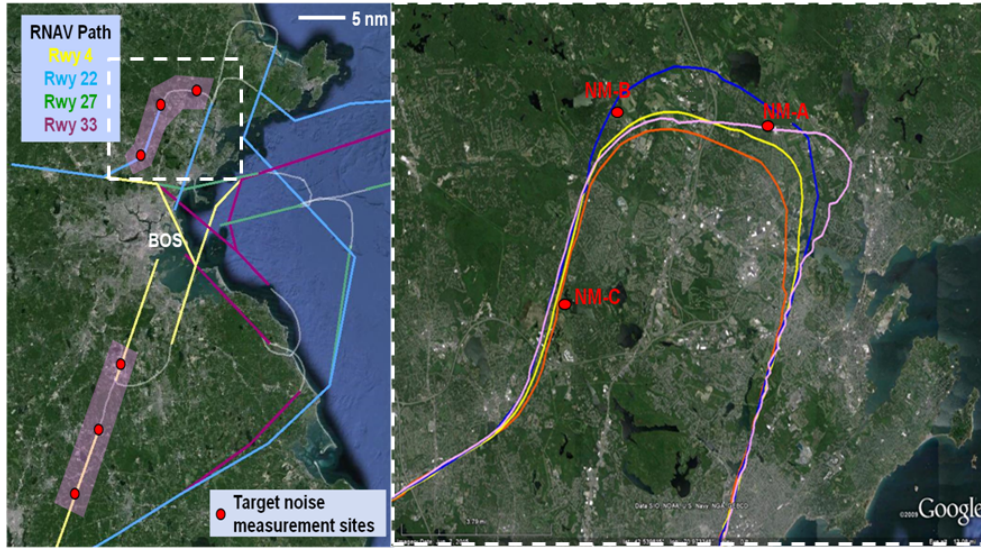
Figure 22: Initial BOS Targeted and Actual Noise Measurement (NM) Locations

Samples of the measured noise results at each monitor taken from the three most common aircraft types seen in the data, the A320, B737 and E190, are shown below in *Figure 23*. In all of these results, the airspeed shown is the indicated airspeed and the SEL values have been normalized for slant range. Each column is one noise monitor, from least to greatest distance to the runway, and each row represents one of the aircraft types. There is a 10-15 dB variability in the noise levels that spans across all the airspeeds. Discussions with aircraft noise experts reveal this variability is typical.
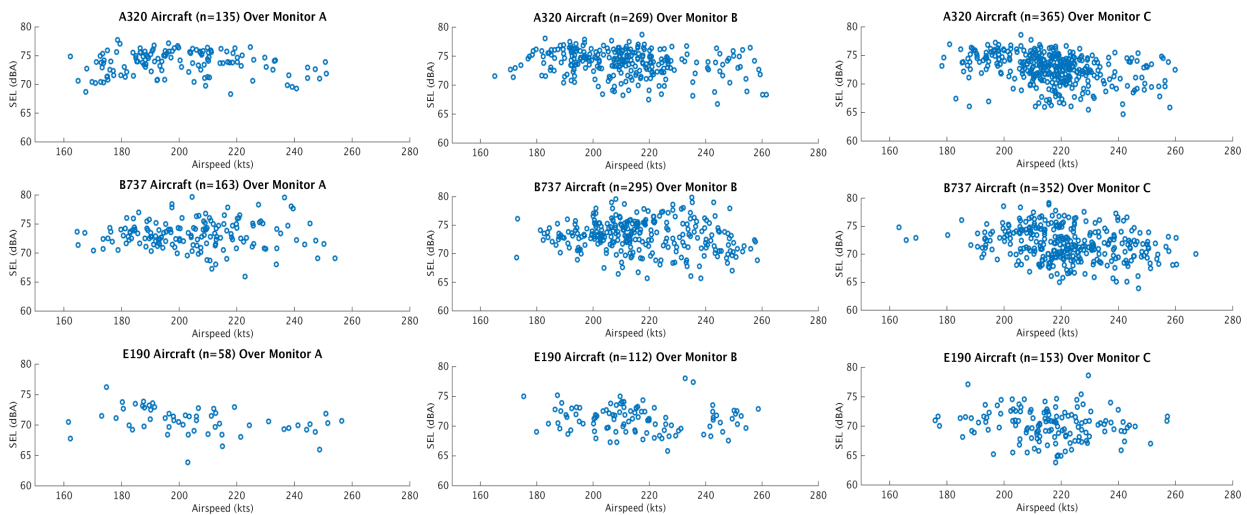
Figure 23: SEL to Airspeed Comparison by Monitor Location & Aircraft Type [25]

With the noise measurement data obtained, the improved noise modeling approach was then used to model example flights from the radar track data analysis in order to validate how well modeled results agree with the measured noise data. For two aircraft types, the A320 and B737, example flights from the BOS noise measurement campaign were chosen based on their average speeds and the number of noise monitors the aircraft flew over. First, the flights with the lowest and highest 5% of average airspeeds were selected. From those subsets, one flight was chosen

that followed a large fraction of the QUABN3 RNAV approach procedure seen in *Figure 22* and flew over at least two noise monitors.

The lateral track, altitude and indicated airspeed of the selected flights were processed through the model in order to develop noise contours. The flap configuration changes were governed by the weight and speed windows for each aircraft type (assuming the flap speed ranges shown in *Table 4*) and the landing gear was assumed to be deployed at 2000 ft.

Boeing 737-800 Flap Speed Ranges (kts)		Airbus A320 Flap Speed Ranges (kts)	
Flaps 1	210 – 250	CONF 1	210 – 230
Flaps 5	200 – 250	CONF 2	180 – 200
Flaps 10	190 – 210	CONF 3	165 – 185
Flaps 15	170 – 200	FULL	155 – 177
Flaps 25	160 – 190		
Flaps 30	150 – 175		

Table 4: Flap Speed Ranges Used for Each Aircraft Type. Max Values Obtained from Flight Crew Operating and Training Manuals for Each Type [27]*,* [28]

The results for an example A320 with an approximately 20 nmi downwind are shown in *Figure 24*. *Figure 24* (a) shows the altitude, airspeed, and modeled thrust settings for the aircraft by distance to touchdown. Plotted on top of the airspeed are the locations where the flap settings changed. *Figure 24* (b) shows the actual flight trajectory, the locations of the noise monitors and the contour of the noise created by that aircraft. As a point of reference, the last three fixes on the QUABN3 RNAV procedure have been plotted, together with markers indicating every 5 nautical miles along the flight track.
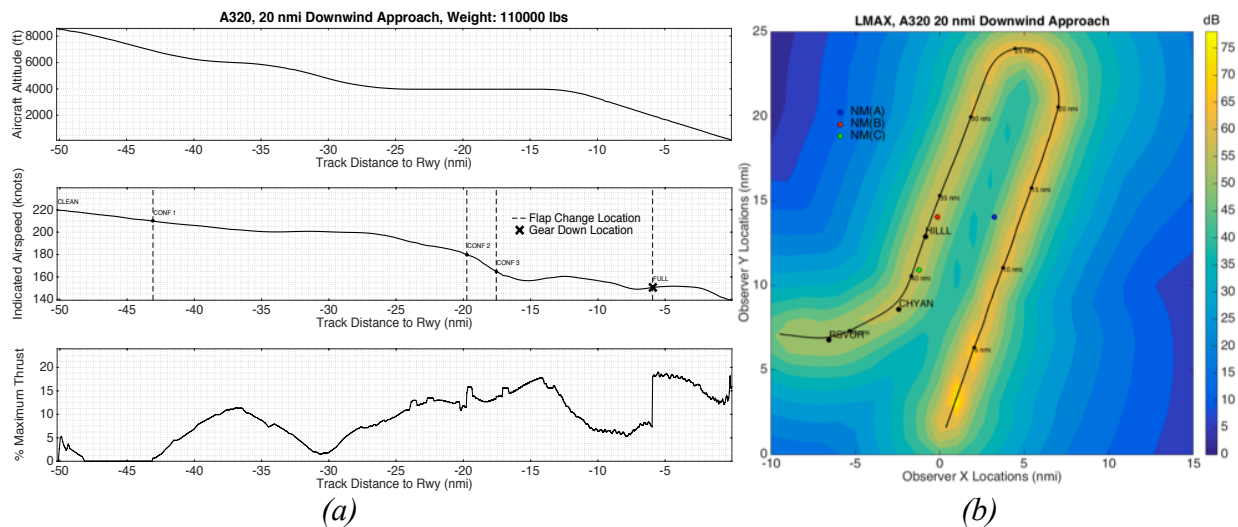
Figure 24: A320 Extended Downwind Approach Flight Profile (a) and LA$_{max}$ Contour (b)

As a comparison, the same analysis was done for an example A320 flight on an approximately 10 nmi downwind approach with the results shown in *Figure 25*. Many of the higher average speed cases were flying this shorter downwind leg, as opposed to an extended one. The thrust settings for this 10 nmi downwind case are at near-idle thrust levels up until the final approach fix where the flap and gear begin extending, whereas in the extended downwind

cases that have earlier decelerations and flaps extended earlier, the thrust levels are increased for the whole flight.

(a)   (b)
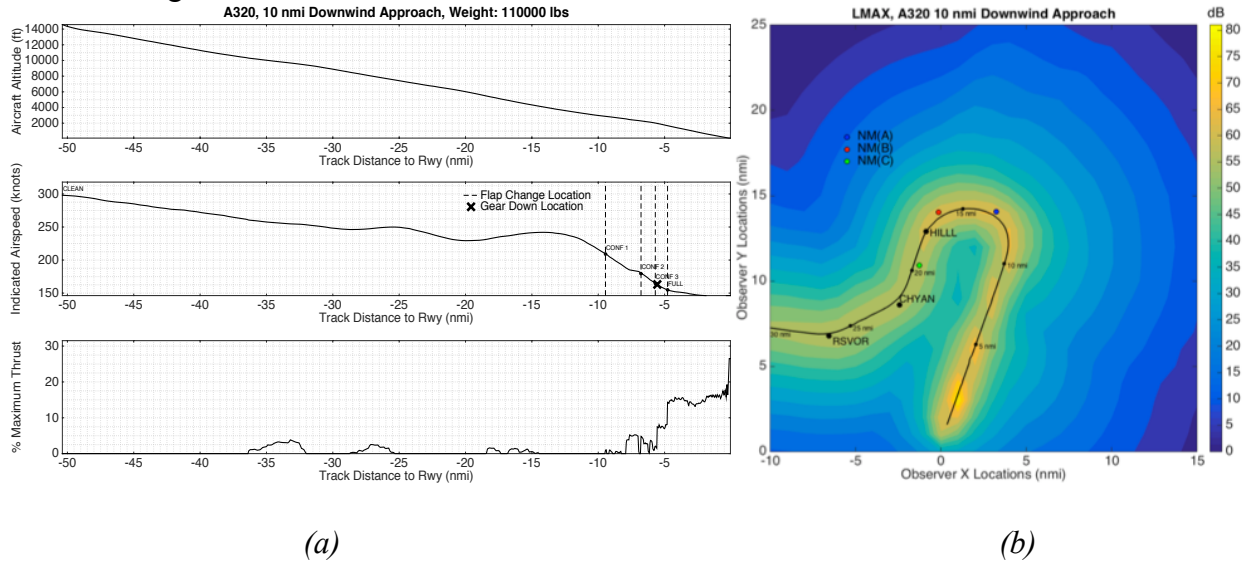
Figure 25: A320 Standard Downwind Approach Flight Profile (a) and LA$_{max}$ Contour (b)

This model was also run for a 10 and 20 nmi downwind profile of a B737-800, with results shown in *Figure 26*. Speed and thrust levels for these cases followed similar trends as with the A320.

(a)   (b)
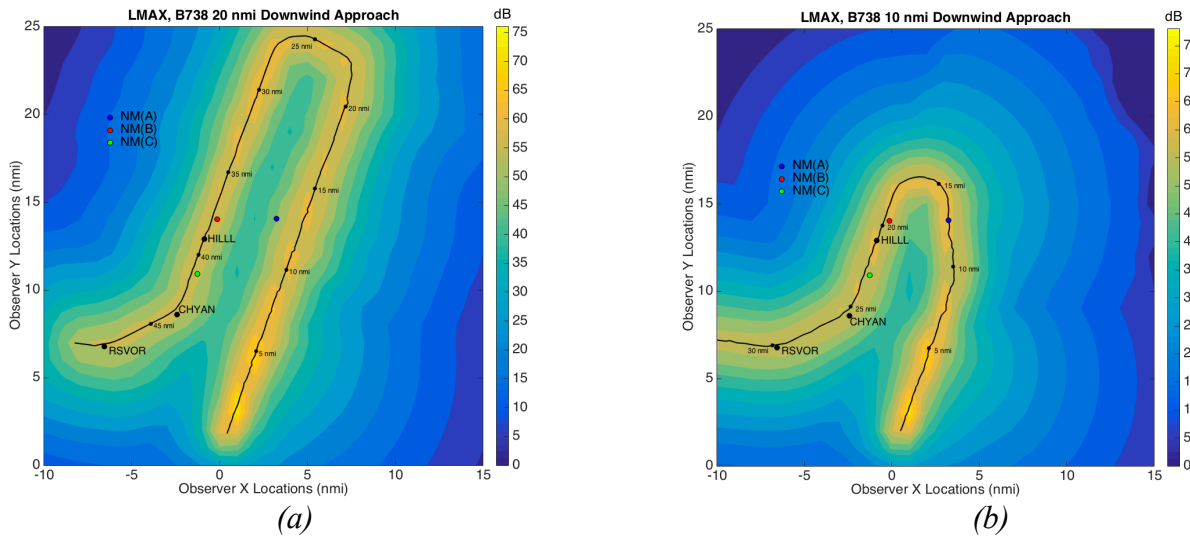
Figure 26: B737 Extended (a) and Standard (b) Downwind Deceleration LA$_{max}$ Noise Contours

The computed values of LA$_{max}$ from the noise contours as the aircraft passes over each noise monitor are shown in *Table 5*. Those values are compared with the measured values recorded by the noise monitors. Comparisons between the measured and modeled LA$_{max}$ data at these locations are within 7 dBA agreement across all cases, i.e., well within the scatter seen in the measured data. Consultation with noise modeling experts in academia, at aircraft manufacturers, and at NASA provided insight about the cause the large scatter in noise measurement results.

Two primary factors influence the variation, and should be taken into account when modeling noise from observed radar data in future examples:

1. Thrust differences between aircraft flying the same published approach based on pilot technique and aircraft energy state.

2. Differences in sound propagation due to atmospheric conditions, shielding in the vicinity of the observer on the surface, wind, etc.

LA_{max} (dBA)	NM (A)		NM (B)		NM (C)		Difference (Measured minus Modeled)		
	Measured	Modeled	Measured	Modeled	Measured	Modeled	NM(A)	NM(B)	NM(C)
20 nmi Downwind A320	-	-	62.38	57.33	60.95	56.57	-	5.05	4.38
10 nmi Downwind A320	61.85	63.97	-	-	54.27	57.65	-2.12	-	-3.38
20 nmi Downwind B737	-	-	59.10	57.76	60.70	55.64	-	1.34	5.06
10 nmi Downwind B737	69.02	62.35	66.50	62.30	60.08	58.89	6.67	4.2	1.19

Table 5: Comparison of Measured and Modeled LA_{max}(dBA)

4.3 Model Limitations

The improved noise analysis method is not without some limitations that must be addressed for each modeling case:

- Some noise unique noise signatures specific to particular aircraft may not be fully captured in ANOPP. For example, ANOPP does not compute noise due to speedbrakes. Unique noise signatures such as these can be added to the total ANOPP noise computation if the data for that additional noise source is available, however.
- Presently, TASOPT is currently unable to model the drag due to aircraft configuration. This information must be supplemented by data from sources such as BADA 4, and thus assumptions for the drag due to configuration of future aircraft must be made to assess their noise.
- The assumptions made in TASOPT's physics-based weight computations limits its airframe sizing to "tube and wing" style aircraft configurations. Thus, to assess aircraft that do not follow these configurations, the sizing of these aircraft must occur externally to the TASOPT methods.

5 Case Study 1: Use of the Improved Noise Analysis Method to Evaluate Noise of a Single Event Advanced Operational Flight Procedure with Complex Airspeed and Configuration Setting Changes

This section presents a case study that was chosen to demonstrate the use of the improved noise analysis method in analyzing the noise impacts of an advanced operational flight procedure with complex airspeed and configuration setting changes. This particular analysis requires modeling methods that can capture the noise effects of airspeed and configuration settings, a capability that is not available in the AEDT method where NPD curves that are used for noise data interpolation are referenced to set configurations and an airspeed of 160 kts. This is a capability that the improved noise analysis method, which uses ANOPP as its noise model and thus enables engine and airframe noise to be computed independently of each other, is designed to accomplish as an improvement of current noise analysis methods.

5.1 The Delayed Deceleration Approach (DDA) Procedure

The first case study performed that demonstrated the usage of the improved noise analysis method is the evaluation of the noise impact of an advanced operational flight procedure: the delayed deceleration approach (DDA). In conventional approaches, the aircraft decelerates and becomes fully configured relatively early in the approach. This results in the aircraft needing thrust to account for the increased drag due to being fully configured. In contrast, delayed deceleration approaches are such that the aircraft delays its deceleration and subsequent release of flaps and gear until later in the approach, as shown in *Figure 27*. The thrust needed to counteract the increased drag due to being fully configured thus occurs over less of the total flight profile than in the conventional approach case.
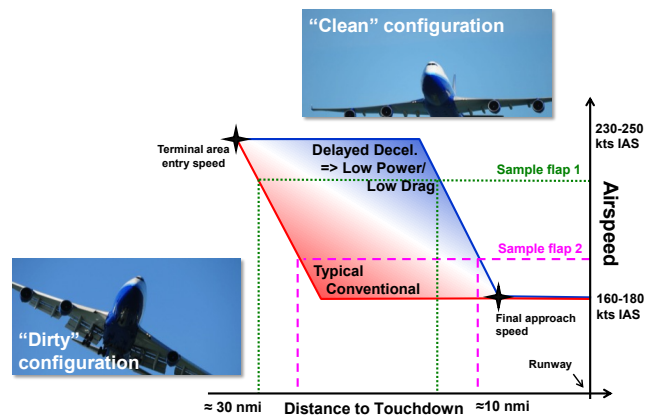
Figure 27: Speed Profiles for Conventional (Red) and Delayed Deceleration (Blue) Approach Profiles [25]

The overall reduction in required thrust, as well as the reduced flight time needed to fly the same distance due to a higher velocity being maintained for most of the flight profile, has been proven to result in a reduction in fuel burn compared to a conventional approach profile [29], as shown in *Figure 28*, making them an attractive procedure for fuel burn savings. It is not clear upon initial observation however what the noise impacts of delayed deceleration approaches are;

compared to a conventional approach, the thrust reductions result in decreased engine noise while the higher speed results in increased airframe noise. It was thus desirable to analyze these effects using the improved noise modeling approach that can capture both the noise effects of the engine and airframe individually.
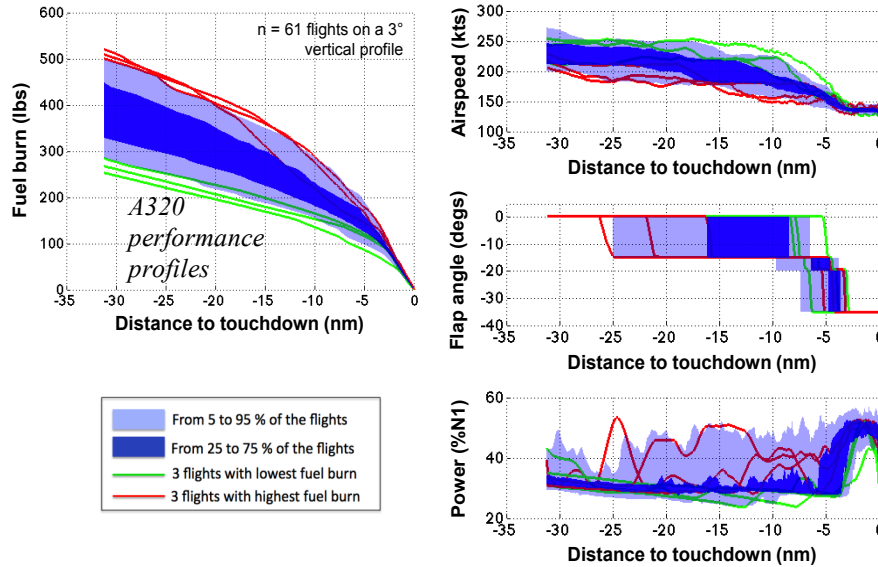
Figure 28: European A320 Flight Data Recorder Analysis (similar for B757 & B777) [29]

5.2 Modeling of Enhanced DDA Operations

The noise effects of employing delayed deceleration approaches on two example theoretical flight profiles were computed first. In these examples, a Boeing 737-800 flying a straight in approach at maximum landing weight (to maximize noise impacts) was modeled. The first example in *Figure 29* shows the effects of employing an early deceleration and delayed deceleration on a sample conventional approach profile as computed by the flight profile generator. As seen *Figure 29* (a), both flights maintain the same altitude of 2000 feet until localizer intercept at the final approach fix, after which the gear comes down and both aircraft descend to the runway. However, in the early deceleration case, the aircraft decelerates at the idle thrust setting provided by BADA 4 from 240 kts at the beginning of the profile until it reaches the final approach speed. It maintains that speed until the final approach fix. For the delayed deceleration case, the aircraft maintains a speed of 240 kts as long as possible and then decelerates at idle thrust to the final approach speed. From the final approach fix on, the speed profiles are identical. The thrust profiles show that, except for when the early deceleration case is at idle thrust during the initial deceleration, the thrust is lower for the delayed deceleration case as expected.
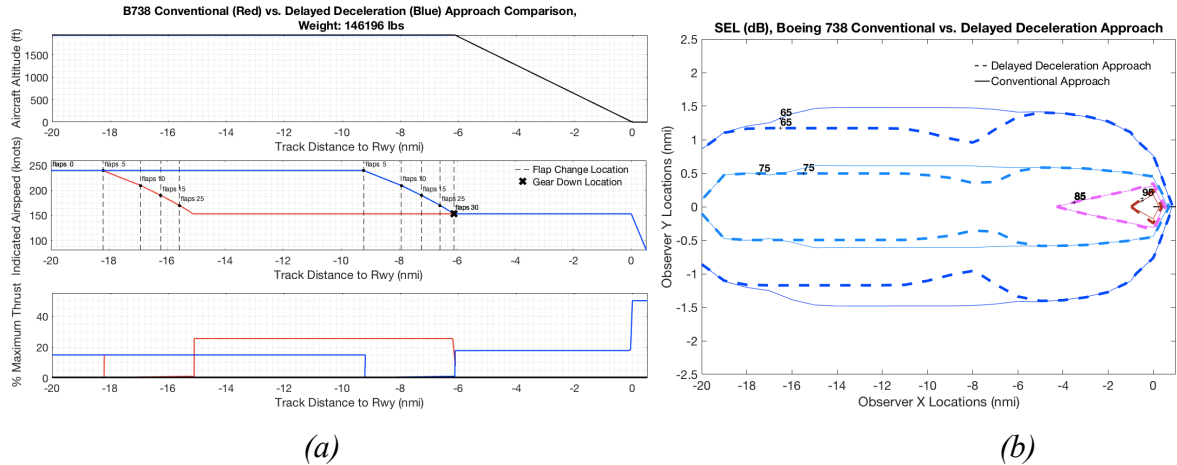
Figure 29: Altitude, Velocity, and Thrust Profiles (a) and SEL Contours (b) of an Early and Delayed Deceleration Conventional Approach Profile

Noise contours were calculated for each profile, with SEL chosen as the metric to capture event duration effects. The SEL contours of the early and delayed deceleration cases of the conventional approach profile are overlaid in *Figure 29* (b). In this example, the early deceleration case is as loud or louder in all regions than the delayed deceleration case. It is apparent that the reduction in thrust and resulting engine noise over much of the delayed deceleration profile is greater than the increase in airframe noise that results from the increased speed. This is evident when looking at the SEL contours of the airframe noise only (*Figure 30* (a)) and the engine noise only (*Figure 30* (b)). Thus in this example, the delayed deceleration case provides a marginal noise benefit compared to the early deceleration case.
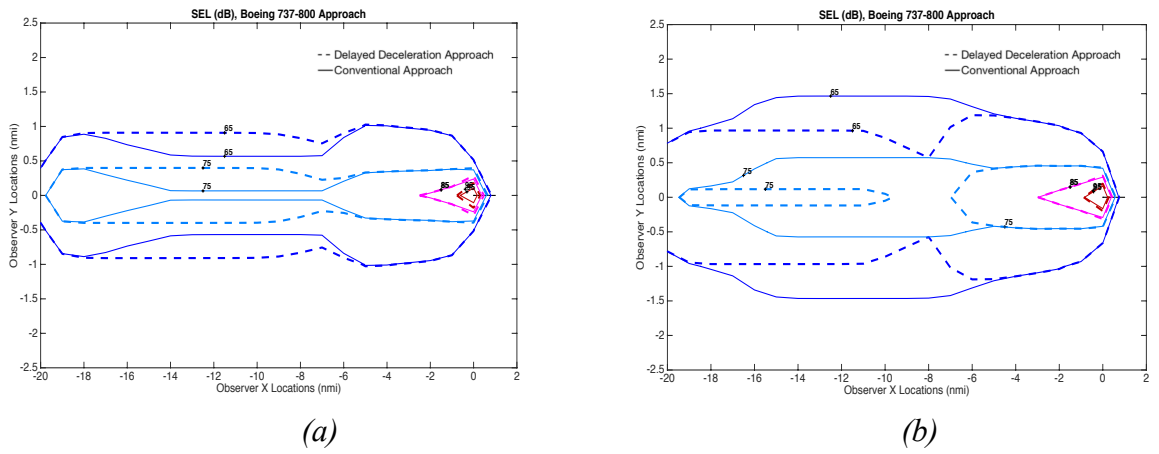
Figure 30: SEL Contours of an Early and Delayed Deceleration Conventional Approach Profile, Airframe Noise Only (a) and Engine Noise Only (b)

The second example in *Figure 31* shows the effects of employing an early deceleration and delayed deceleration on a continuous descent profile. In the early deceleration case, the aircraft again decelerates at the idle thrust setting from 240 kts at the beginning of the profile until it reaches the final approach speed, while in the delayed deceleration case, the aircraft maintains a speed of 240 kts as long as possible and then decelerates at idle thrust to the final approach speed. From the final approach fix on, the speed profiles are again identical. The thrust profile

41

again shows that except for when the early deceleration case is at idle thrust during the initial deceleration, the thrust is lower for the delayed deceleration case as expected. However, the difference in thrust between the early and delayed deceleration cases is less than in the conventional approach example.
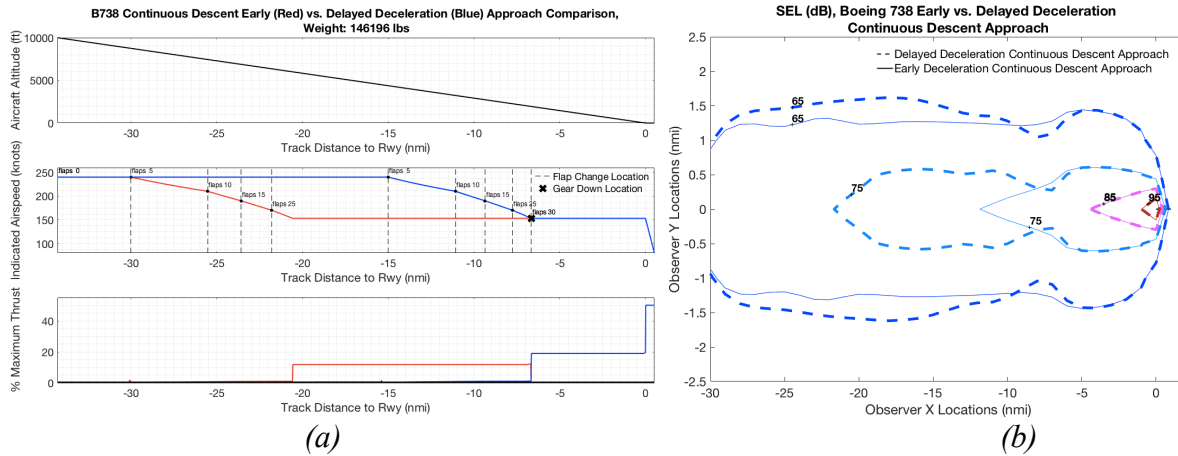
Figure 31: Altitude, Velocity, and Thrust Profiles (a) & SEL Contours (b) of an Early and Delayed Deceleration Continuous Descent Profile

The SEL contours of the early and delayed deceleration cases of the continuous descent approach profile are overlaid in *Figure 31* (b). Unlike the conventional approach example, the delayed deceleration case in this example is as loud or slightly louder in all regions than the early deceleration case. In this case the increase in airframe noise that results from the increased speed reduction in the delayed deceleration profile is greater than the reduction in thrust and resulting engine noise. This is again evident when looking at the SEL contours of the airframe noise only (*Figure 32* (a)) and the engine noise only (*Figure 32* (b)). Thus in this example, the delayed deceleration case provides a small noise detriment compared to the early deceleration case.
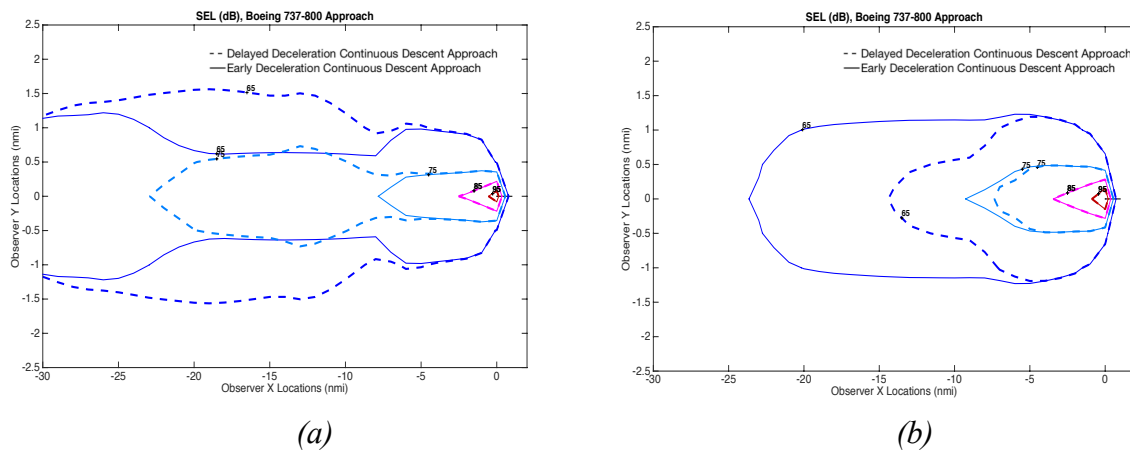
Figure 32: SEL Contours of an Early and Delayed Deceleration Conventional Approach Profile, Airframe Noise Only (a) & Engine Noise Only (b)

5.3 Modeling of Enhanced DDA Operations at Boston Logan Airport (BOS)

The improved noise modeling approach was lastly used to examine the effects of employing a delayed deceleration approach on a flight track into BOS following the QUABN3 RNAV into runway 22L (introduced in section 4.2) and comparing it directly with an early deceleration case. The A320 20 nmi downwind case in *Figure 24* (in section 4.2) and *Figure 33* (b) was used to represent a sample early deceleration profile. The same altitude and lateral profile as well as wind conditions of this flight track were then used to create an early deceleration case where the aircraft starts decelerating at the start of the profile at idle thrust until it reaches the speed at the final approach fix of 150kts. Flaps are assumed to change at the maximum flap speeds from in *Table 4* (in section 4.2) in order to compute the shortest length needed to decelerate. Similarly, a delayed deceleration case where the aircraft maintains its initial speed of 220kts as long as possible and then decelerates at the idle thrust setting to the final approach speed is also modeled. From the final approach fix on, the speed and thrust profiles of both cases are identical.

The altitude, speed, and thrust profiles are overlaid and shown in *Figure 33*, where red represents the early deceleration case and blue represents the delayed deceleration case. Aside from the start of the profile where the early deceleration case is at idle thrust, the computed thrust for the delayed deceleration case is generally lower as expected.

(a)   *(b)*
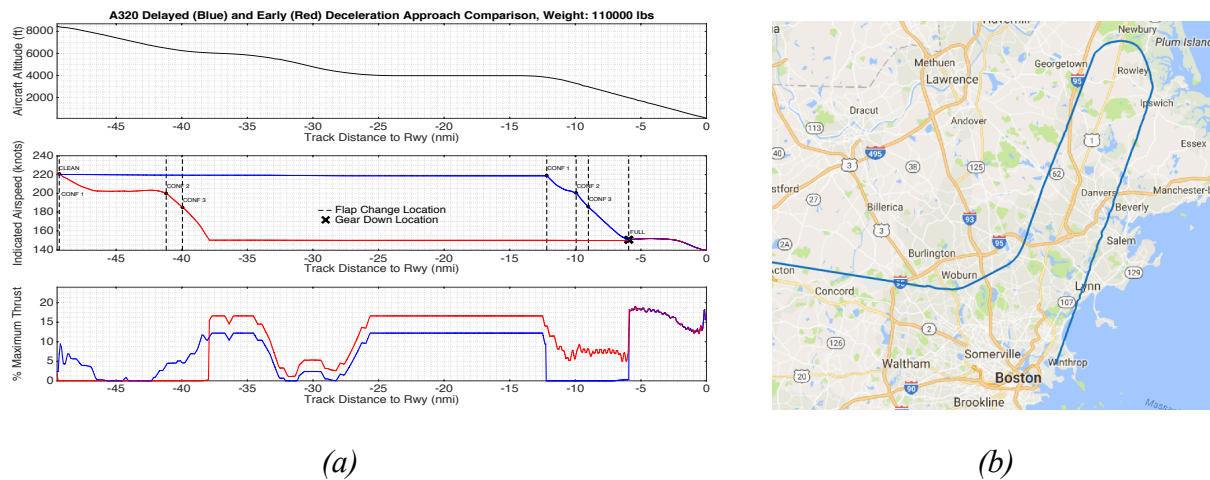
Figure 33: Delayed (Blue) and Early (Red) Deceleration Flight Profiles (a) & Flight Track into BOS from Flight Recorder Data (b)

The difference in SEL generated by the delayed and earliest deceleration flight profiles is shown in *Figure 34*, where red indicates the delayed deceleration approach is louder and blue indicates the early deceleration case is louder. The noise results in *Figure 34* (a) show that while SEL is decreased to the left and right of most of the flight path for the delayed deceleration case, noise is also increased directly under most of the flight path. It is apparent that the increase in airframe noise due to the increased speed for most of the delayed deceleration case is greater than the decrease in engine noise resulting from the reduced thrust for most of the profile. This is again evident when looking at the SEL contours of the airframe noise only (*Figure 34* (b,i)) and the engine noise only (*Figure 34* (b,ii)). Similar to the continuous decent delayed deceleration approach example in the previous section, the delayed deceleration case provides a small noise detriment compared to the early deceleration case.
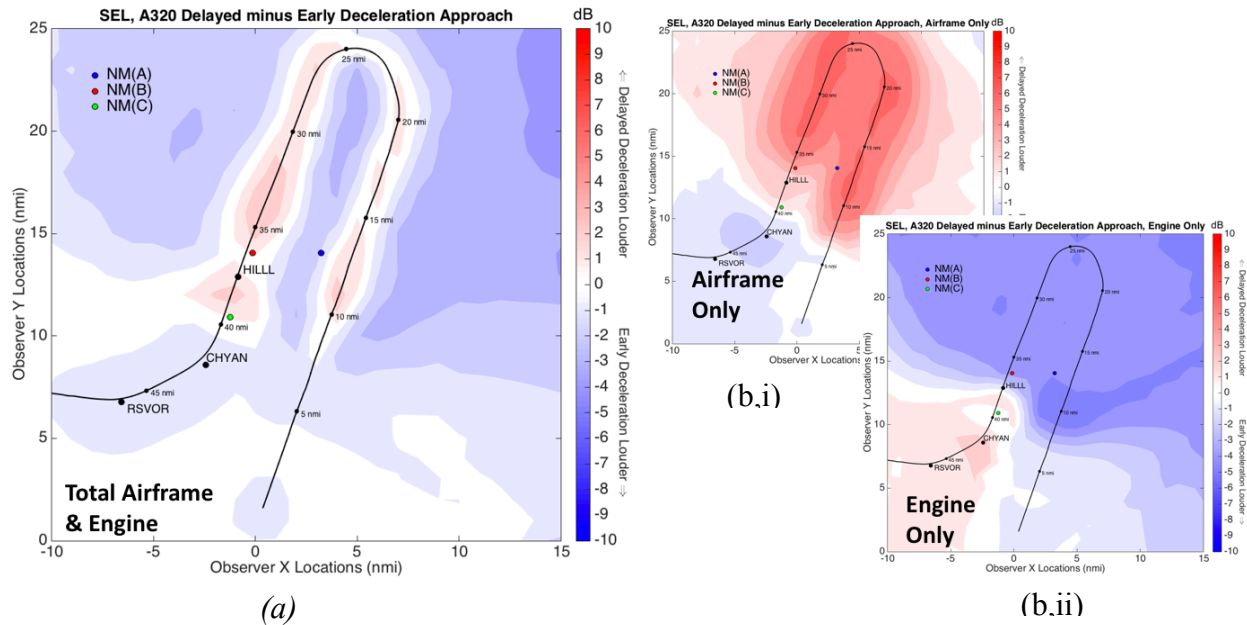
Figure 34: Difference in Computed SEL (Delayed Deceleration minus Early Deceleration), Total Noise (a) & Airframe Noise Only (b,i) and Engine Noise Only (b,ii)

5.4 Conclusion

The improved noise modeling approach was used to assess the noise impacts of DDAs as a demonstrator of its capability to assess single-event advanced operational flight procedures. One impediment that was not well understood about DDAs was their impact on noise levels. The procedures typically result in lower engine thrust settings (and hence lower engine noise) but higher airspeeds (and hence higher clean airframe noise) early in the approach, but potentially slightly higher engine thrust and greater high-lift device usage later in the approach such that the net effect is unclear.

The examples shown in this case-study demonstrate the differing roles of airframe and engine noise at various points along the approach path with a range of speed profiles. The results of the improved noise modeling approach showed employing DDA's in flight procedures where thrust already relatively low, such as continuous descent approaches, may not be beneficial for noise because the decreased engine noise from the low thrust of DDA's is not enough to counter the increased airframe noise from high speeds of DDA's. The results of this case study also show that the noise difference of a DDA and a conventional approach is within the data scatter seen in typical noise monitor data, such as that presented in section 4.2. Follow up work in this area is more careful optimization of the speed profiles and timing of when to put down flaps and gear for minimum noise.

44

6 Case Study 2: Use of the Improved Noise Analysis Method to Evaluate Fleet Level Noise of Future Aircraft

This section presents a case study that was chosen to demonstrate the use of the improved noise analysis method in analyzing the noise impacts of future aircraft. This particular analysis requires modeling methods that can capture the noise effects of future aircraft for which there does not exist flight test data, a capability that is not available in the AEDT method where NPD curves that are used for noise data interpolation are built from existing-aircraft flight test data. This is a capability that the improved noise analysis method, where one can design a future aircraft in TASOPT and obtain its performance and geometry for input into ANOPP, is designed to accomplish as an improvement over the current methods.

6.1 Aircraft Upgauging

The second case study to demonstrate the improved noise analysis method is modeling the noise impact of a hypothetical future change in the standard aircraft fleet in the form of an aircraft guage policy implementation. Aircraft gauge refers to the size and payload of an aircraft. Increasing average gauge of the aircraft in service and increases the passenger throughput at a given airport.

While a policy requiring all aircraft to be upgauged will result in an increase in passenger throughput at an airport, the effects on community noise around the airport from such a policy are not obvious. An upgauged aircraft will have different engine performance and airframe geometry than its baseline, both of which are critical factors to the overall noise of the aircraft, and the extent of that change may vary by aircraft type. The need to know the noise characteristics of future, upgauged aircraft for this problem thus makes its analysis using AEDT, which relies on test data of existing aircraft, questionable. This problem is thus a good demonstrator of using component-based noise analysis method to assess noise of future aircraft. In this example, the noise impact of increasing a baseline sample fleet of aircraft at Reagan National Airport (DCA), shown in *Figure 35* (b), by a 10% upgauged fleet is analyzed and compared to a representative baseline fleet.
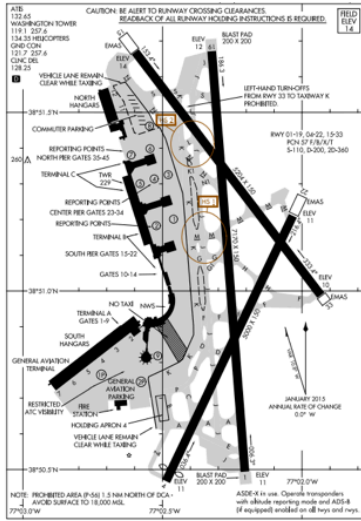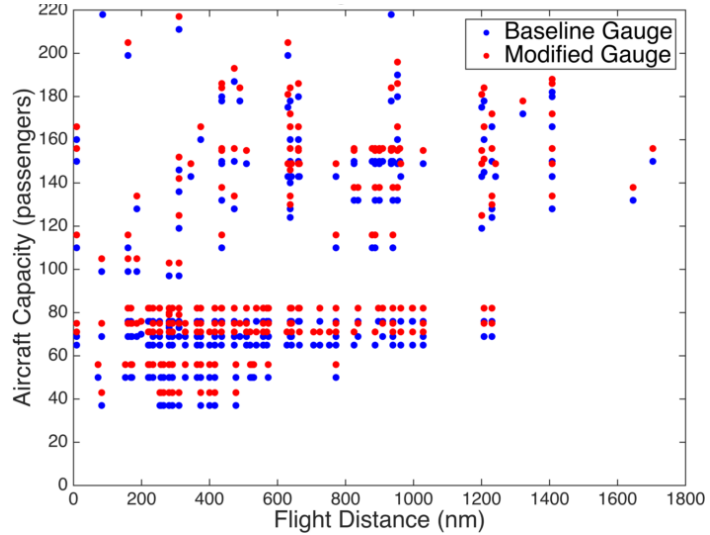
(a)   *(b)*

Figure 35: Airport Layout at DCA [30] (a) & Demonstration of Passenger Capacity Increase via 10% Upgauge during the Week of August 2, 2015 at DCA (b)

The chosen metric to assess the noise impact of a 10% upgauge policy at DCA is the day night average sound level (DNL) metric. This metric was chosen because it represents the cumulative noise of all aircraft operations at an airport averaged out over a 24-hour period. DNL requires an SEL contour of every aircraft operation during that time period. Therefore both the aircraft types (i.e., their performance characteristics) and their four-dimensional flight profiles (altitude, speed, thrust, lateral position) versus time are needed to compute DNL.

6.2 Aircraft Fleet Selection and Modeling in TASOPT

The aircraft fleet chosen for this scenario is a representative day of operations flown into DCA in 2015. *Table 6* contains all aircraft types and quantities in this as given in ASDE-X aircraft flight radar track data for this year. While it is possible using this method to model each aircraft type individually, in this case study to simplify the modeling process, each aircraft was grouped into representative bins based on their aircraft class (for example, the Airbus A320 group and the Boeing 737 group), weight, and passenger count to form six representative aircraft types to represent the entire fleet.

2015 Arrivals by Type at DCA

Type Code	Annual Arrivals	Representative Type	Average Daily Arrivals
E170	28732	E170	132.4
E190	13399		
CRJ7	3734		
CRJ9	2455		
E135	222	E145	94.8
E145	2189		
E45X	1223		
CRJ2	28835		
DH8A	869		
DH8D	586		
GA T-Prop	370		
GA Turbine	290		
A319	16658	A320	65.9
A320	6419		
A321	985		
B733	193	B738	83.6
B737	15512		
B738	14684		
B739	117		
B752	814	B752	2.2
B712	378	MD88	16.6
MD82	22		
MD83	11		
MD88	2546		
MD90	3095		
Heli+Light GA	Omitted	Omitted	–
Total			**395.4**

Table 6: Number of Aircraft Operations Flown Into DCA in 2015 & Final Grouping of Aircraft Types into Bins

Table 6 shows that the representative fleet of this example day consists of the A320, B738, B752, E145, E170, and MD88. Each of these are then modeled in TASOPT to create the baseline aircraft fleet. A baseline TASOPT aircraft model is generated in TASOPT given:

- Mission requirements (max range, cruise altitude, cruise Mach number, design load limits, and number of passengers).
- Geometry requirements (the sweep, taper, thickness to chord, and aspect ratio of the wings and tails, the tail volume coefficients, the length and diameter of the fuselage, and the wing airfoil)
- Weight ratios of aircraft components
- Engine technology level parameters (max turbine inlet temperature at takeoff, pressure ratios and efficiencies of the engine stations, and design bypass ratio).

To model the upgauged TASOPT aircraft, the number of passengers was increased by 10% and the length of the fuselage was increased by 10%, as shown in *Figure 36*. With all other inputs held constant, the aircraft wing, tails, and engines were then resized to compensate for the larger payload and fuselage. The new aircraft and engine performance values were also calculated.
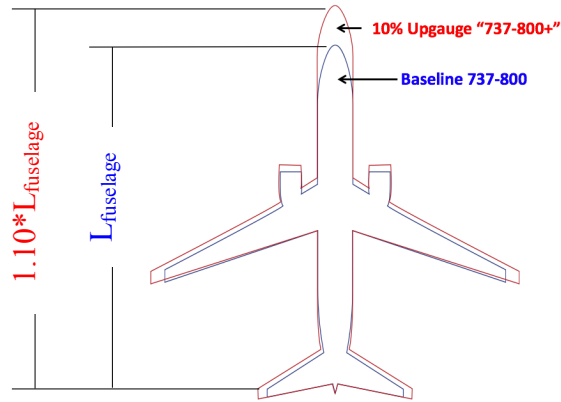
Figure 36: Demonstration of the 10% Upguage of a Boeing 737-800

The final baseline aircraft and their 10% upgauged models are shown in *Figure 37*. Each aircraft has an increased wing area and thus increased tail area to account for the increased weight of the upgauged aircraft with respect to the baseline. The max takeoff thrust of each upgauged aircraft also increased to meet the same top of climb mission requirements as the baseline cases.
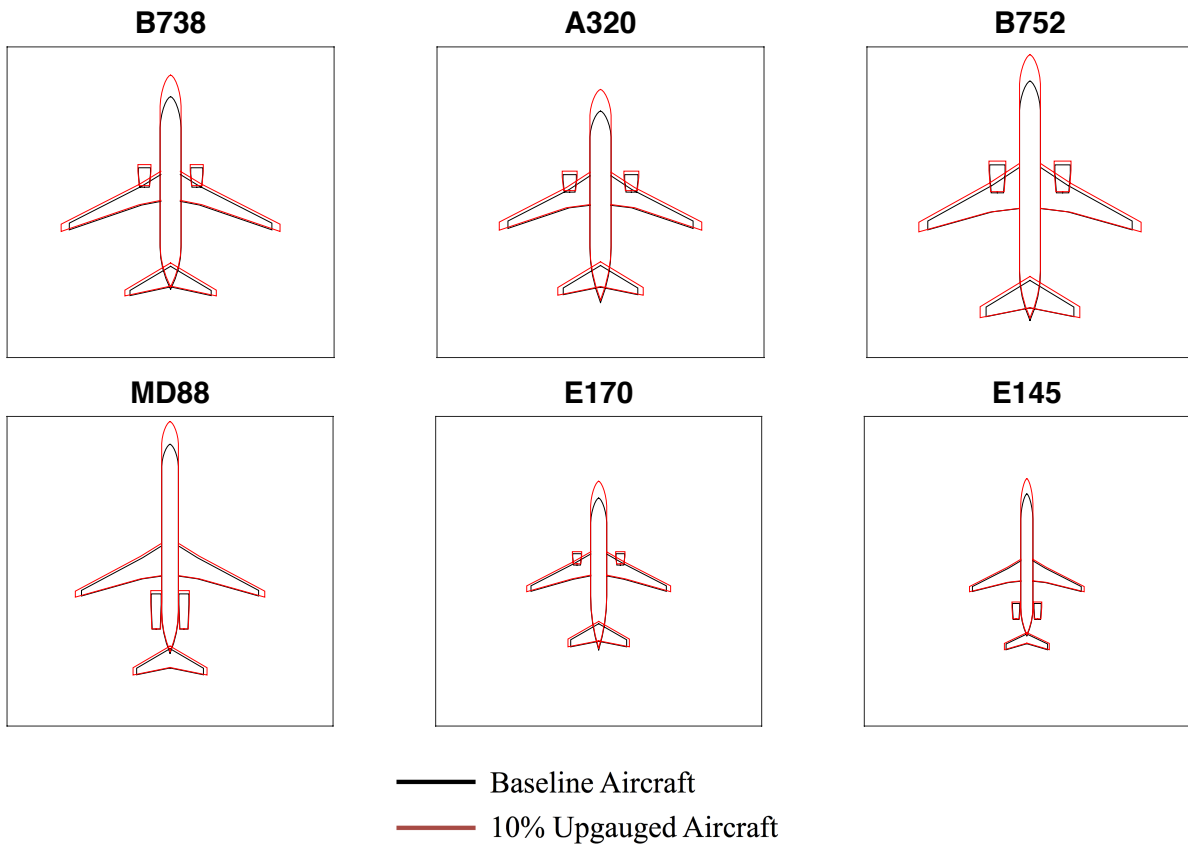
Figure 37: Baseline Fleet and their Upgauges as Computed by TASOPT

6.3 Trajectory Generation using the Flight Procedure Generator

The flight procedure of each aircraft type consists of the lateral track, as well as altitude, speed, thrust per time. This section describes how these procedures were modeled for the aircraft fleet.

6.3.1 Lateral Track Modeling

Rather than model each aircraft flying each individual lateral track that is present at an airport on any given day, a representative set of lateral track definitions for the sample fleet of aircraft was generated based on sample historical ASDE-X aircraft radar flight track data from 20 representative days spread between 2015 and 2016. The data such as that shown in *Figure 38* was filtered to identify which flights flew RNAV routes, after which the chosen route was the lateral track that closest matched the centroid of the flights that flew this RNAV route, as demonstrated in *Figure 39*. As can be seen in *Figure 39* (c) and (d), six departures and four arrivals were identified from this method.
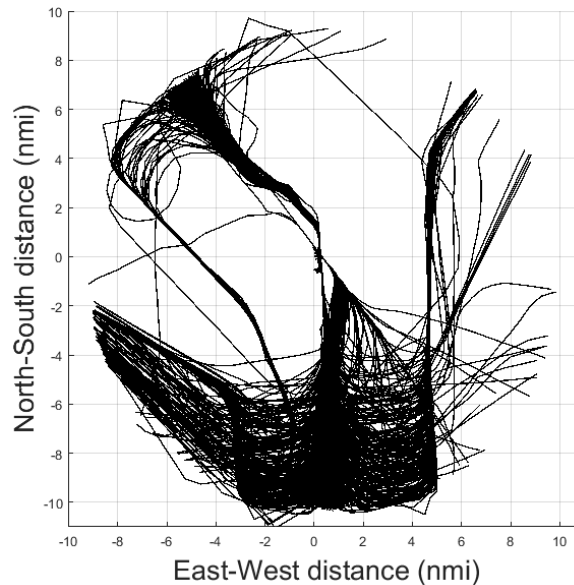
Figure 38: Sample ASDE-X Flight Track Radar Data at DCA before Filtering to Identify RNAV Routes, figure by Callen Brooks[1]
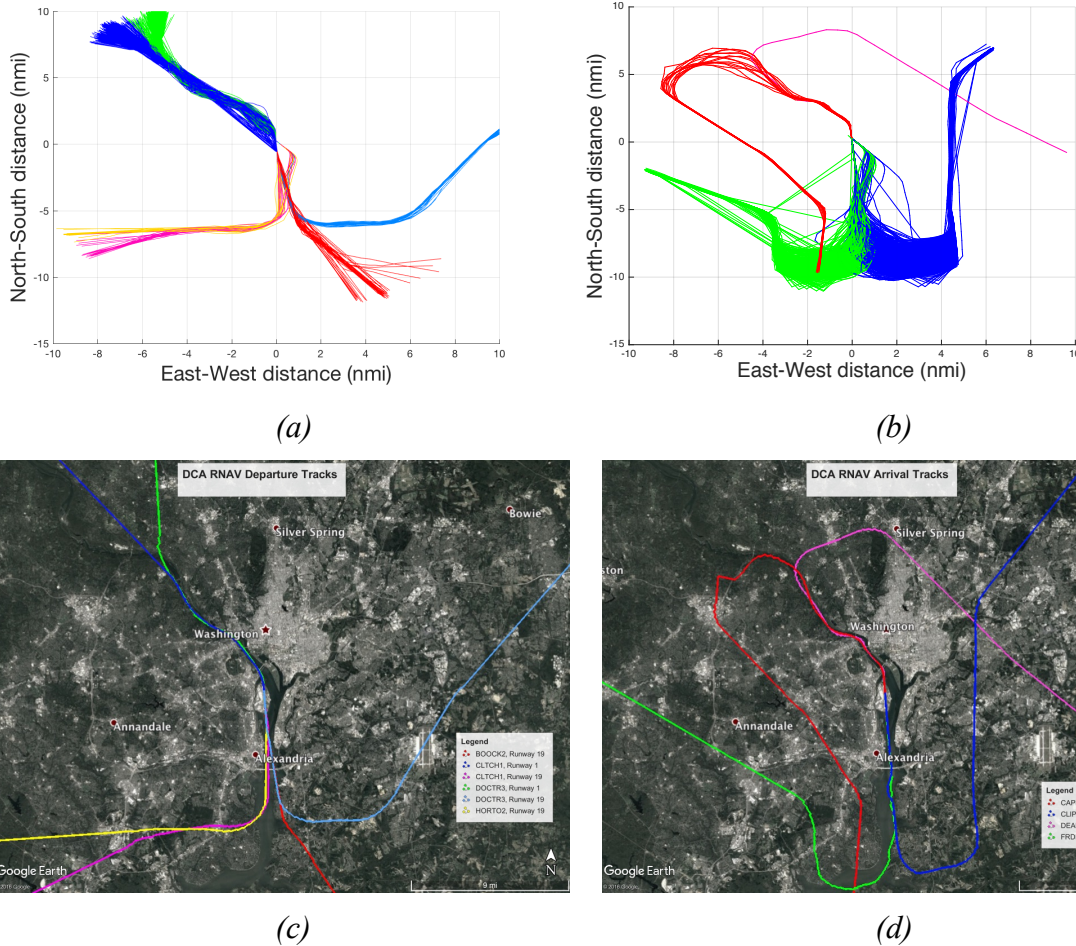
Figure 39: DCA Departure (a) & Arrival (b) ASDE-X Flight Track Radar Data Filtered for RNAV Routes and Final Departure (c) & Arrival (d) Centroid Routes, figures by Callen Brooks[1]

6.3.2 Configuration and Drag Modeling

The altitude, position, and thrust profiles were obtained using the flight profile generator for all baseline and upgauged aircraft types. The upgauged aircraft were assumed to have the same flap settings as the baseline aircraft. For example, both the A320 and A320 "upgauge" have flap settings CONF 1, CONF 2, CONF 3, and FULL with the same speed ranges as shown back in *Table 4*. Because, as mentioned in section 3.1.4, TASOPT at the time of this analysis does not provide a detailed drag estimate for aircraft flap and gear configurations, an estimate had to be made about the incremental drag increases for the various flap and gear configurations of the upgauged aircraft types. It was assumed that the upgauged aircraft had the same incremental drag polars, available in BADA 4, that are functions of lift coefficient, speed, and configuration as their baseline counterparts. A baseline aircraft and its upgauge would thus have the same drag at the same speed, lift coefficient, and configuration, but particularly because the upgauged aircraft will always be flying at a higher lift coefficient then its baseline because of its higher weight, the computed drag force of the upgauged aircraft is different to be higher than its baseline for any given position along a flight procedure.

A comparison of the total drag coefficients provided by BADA 4 was done to determine the fidelity of this assumption. Each aircraft family shown are nearly 10% stretched versions of each

50

other, with the length of the A320 equal to 111% the length of the A319 [31], [32], the B739 equal to 107% the length of the B738 [33], and the E145 equal to 113% the length of the E135 [34], [35]. Each aircraft within the same family has the same wing. One noticeable trend was that the longer aircraft in general have slightly lower drag coefficients at the same lift coefficient and configuration. The additional drag effects of each of these stretched aircraft did not include the effects of also having a larger wing, as is present in the 10% upgauged aircraft of the DCA case study. It was thus decided that assuming the drag polars of the DCA case study baseline and upgauged aircraft are equal is sufficient to a first approximation, as the additional drag from the larger wing in the upgauged aircraft may offset the apparent slight drag reduction from purely stretching the fuselage that the BADA 4 data shows.

6.3.3 Departure Procedure Modeling

The departure profiles were assumed to notionally follow the International Civil Aviation Organization's Procedure B [36], with details about the specific climb rates and accelerations defined by the standard departure profile definitions from AEDT's standard input file reference guide [37]. *Table 7* summarizes the final representative DCA departure profile definition.

Altitude (ft)	Speed (kts IAS)	Configuration	Thrust
0	0	2nd Setting from clean + gear†	Derated Max TO*
0	V2*	2nd Setting from clean + gear†	Derated Max TO*
1000	V2*	2nd Setting from clean†	Derated Max TO*
As reached at end of acceleration at 2/3 initial climb rate	V2+15*	2nd Setting from clean†	Derated Max TO*
As reached at end of acceleration at 1/2 initial climb rate	V2+25*	1st Setting from clean†	Derated Max TO*
As reached at end of acceleration at climb rate 1000 fpm	V zero flaps†	Clean	Mean Climb#
3000	V zero flaps†	Clean	Mean Climb#
As reached at end of acceleration at climb rate 1000 fpm	250	Clean	Mean Climb#
10000	250	Clean	Mean Climb#

Table 7: DCA Representative Departure Profile Definition

The configuration and speed settings marked by † were obtained from the BADA 4 data for each aircraft type and used for both the baseline and upgauged aircraft. V2 (denoted by *) and

max takeoff thrust are computed by TASOPT for both the baseline and upgauged aircraft separately. The "derated max takeoff" thrust denoted by * and the "mean climb" thrust denoted by # stray from the precise ICAO B departure definition, which specifies maximum takeoff thrust be maintained from start of takeoff to the altitude where the aircraft reaches its 0 flaps configuration velocity and then maximum climb thrust be maintained as the aircraft accelerates from its 0 flaps configuration velocity and continues to climb to 10,000 ft. To represent the departure profiles seen in the ASDE-X flight track radar data more closely, the derated takeoff thrust and mean climb thrust here were instead determined to be that which resulted in a climb gradient that matched the climb gradient of the mean departure profile from ASDE-X flight track radar departure data for each aircraft type. The upgauged aircraft were then assumed to hold the same derate in thrust value as the baseline aircraft. An example of this is illustrated in *Figure 40* (a) and (b). The median departure profiles from these data sets are plotted in white against departure profile data for the E170 baseline and E170 upgauged aircraft. The representative DCA departure profiles for these aircraft are plotted in magenta.

(a) *(b)*
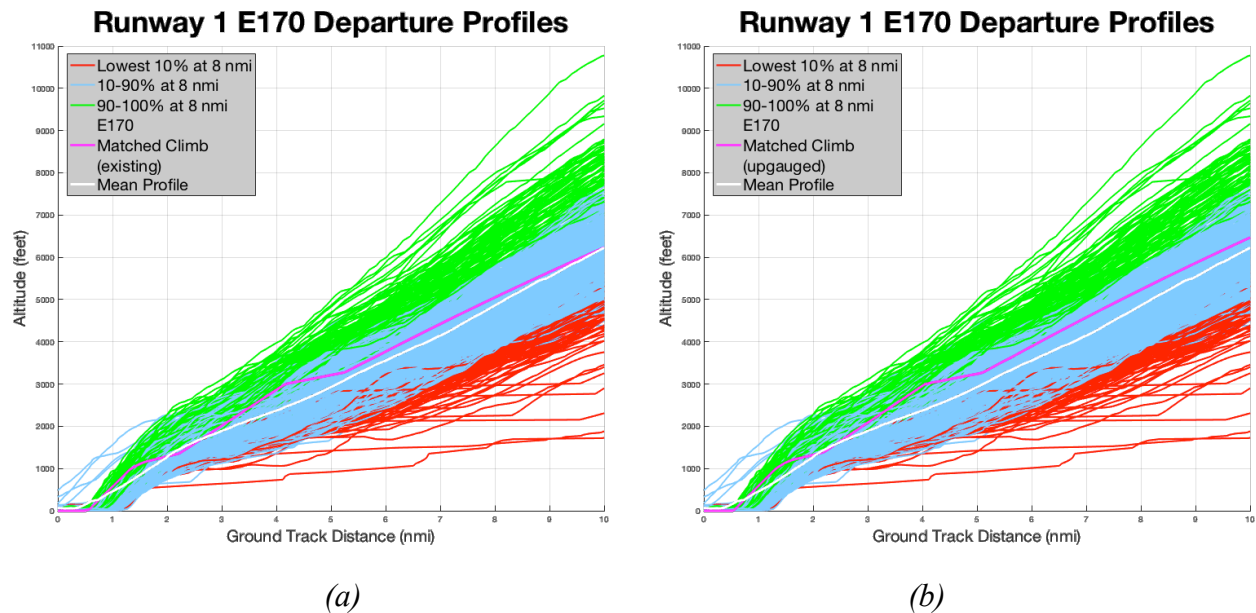
Figure 40: Example of E170 Baseline (a) & Upgauged (b) Departure Profiles Plotted Against ASDE-X Flight Track Departure Data Out of Runway 1 at DCA, figures by Callen Brooks[1]

Two sample baseline and upgauged aircraft altitude, speed, and thrust departure profiles (plotted as % maximum thrust of the baseline aircraft) are shown in *Figure 41*. As expected given the heavier weight of the upgauged aircraft, the thrust profile of the upguaged aircraft are higher than that of the baseline aircraft. This trend is consistent across all aircraft types.

---

[1] Graduate student, Department of Aeronautics and Astronautics at MIT
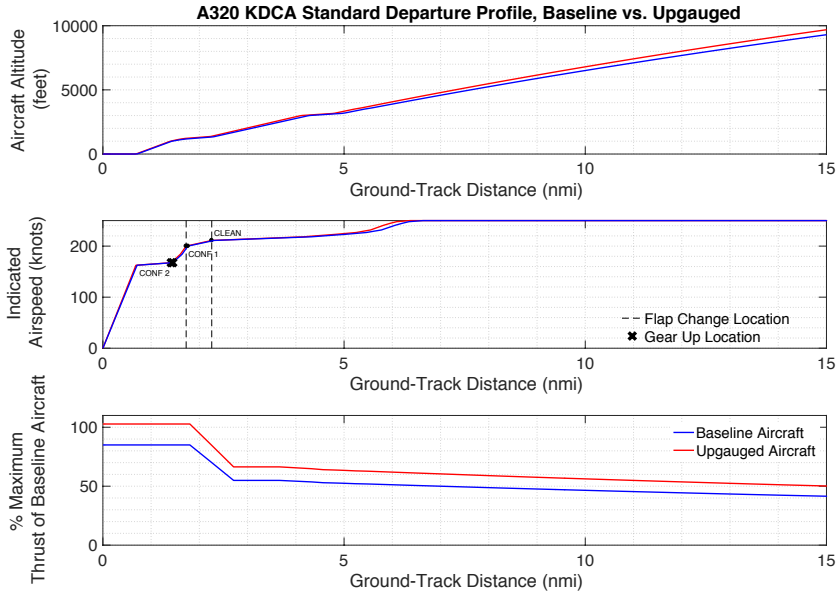
Figure 41: Example of Baseline and Upgauged A320 Departure Altitude, Speed, and Thrust Profiles (Plotted as % Maximum Thrust of the Baseline Aircraft)

6.3.4 Approach Procedure Modeling

Finally, the approach profiles were assumed to be 3° glideslope approaches typical of IFR approaches, starting at 6000 ft with the aircraft at zero-flaps speed and configuration and decelerating from 0 flap speed to final approach speed. The details about the specific flap change locations and accelerations were defined by the standard approach profile definitions described in AEDT's standard input file reference guide [37]. The representative DCA approach profile definitions are summarized in *Table 8*.

Altitude (ft)	Speed (kts IAS)	Configuration	Thrust
6000	250	0	As required
5000:1000:1500	Flap speeds at each altitude†	Flaps change every 1000 ft from 0 to Full Flaps Minus 2†	As required
1500	Approach speed*	Full flaps minus 1 + gear†	As required
1000	Approach speed*	Full flaps + gear†	As required
0	Approach speed*	Full flaps + gear†	%40 Max Static*
0	30	Full flaps + gear†	%40 Max Static*

Table 8: DCA Representative Approach Profile Definition

The configuration and speed settings marked by † were obtained from the BADA 4 data for each aircraft type and used for both the baseline and upgauged aircraft. Approach speed and max static thrust denoted by * are computed by TASOPT for both the baseline and upgauged aircraft separately. *Figure 42* shows this profile for the baseline A320 plotted in magenta against ASDE-

X flight track radar data for common jets arriving into Runway 4. This profile matches closely to the median profile of this data, plotted in white.
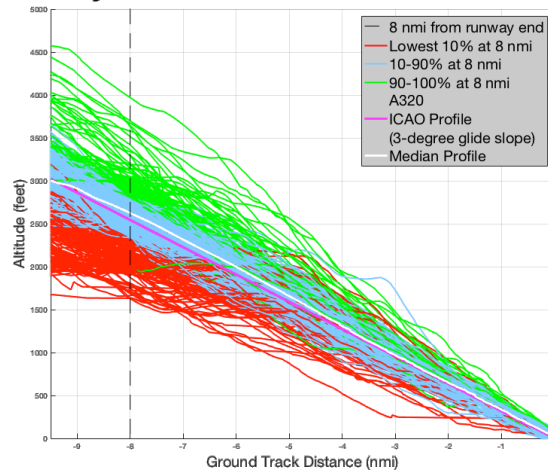
Figure 42: Example of ASDE-X Flight Track Arrival Data Into Runway 4 at DCA, figure by Callen Brooks[1]

Two sample baseline and upgauged aircraft altitude, speed, and thrust arrival profiles (plotted as % maximum thrust of the baseline aircraft) are shown in *Figure 43*. As expected given the heavier weight of the upgauged aircraft, the thrust profile of the upgauged aircraft are higher than that of the baseline aircraft. This trend is consistent across all aircraft types.
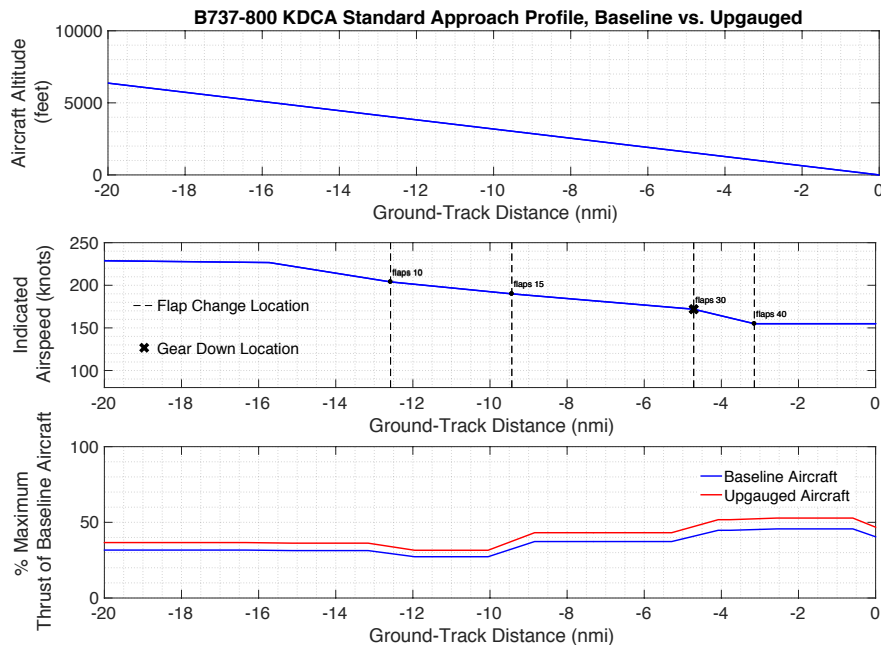
Figure 43: Example of Baseline and Upgauged B738 Arrival Altitude, Speed, and Thrust Profiles (Plotted as % Maximum Thrust of the Baseline Aircraft)

6.4 SEL Noise Results

Given the definitions for both the baseline and upgauged aircraft as well as their flight profiles, described in sections 6.2 and 6.3 respectively, noise results are finally obtained. A few sample arrival SEL plots for aircraft flying arrival 1 that were produced by this method are shown in *Figure 44*. In general, the most of the upgauged aircraft arrivals resulted in louder SEL contours compared to their respective baseline aircraft arrivals; all aircraft groups followed this trend shown in *Figure 44* (a) and (b). This is expected given that the upgauged aircraft are heavier and thus need more thrust to maintain the same glideslope as their baseline counterparts.
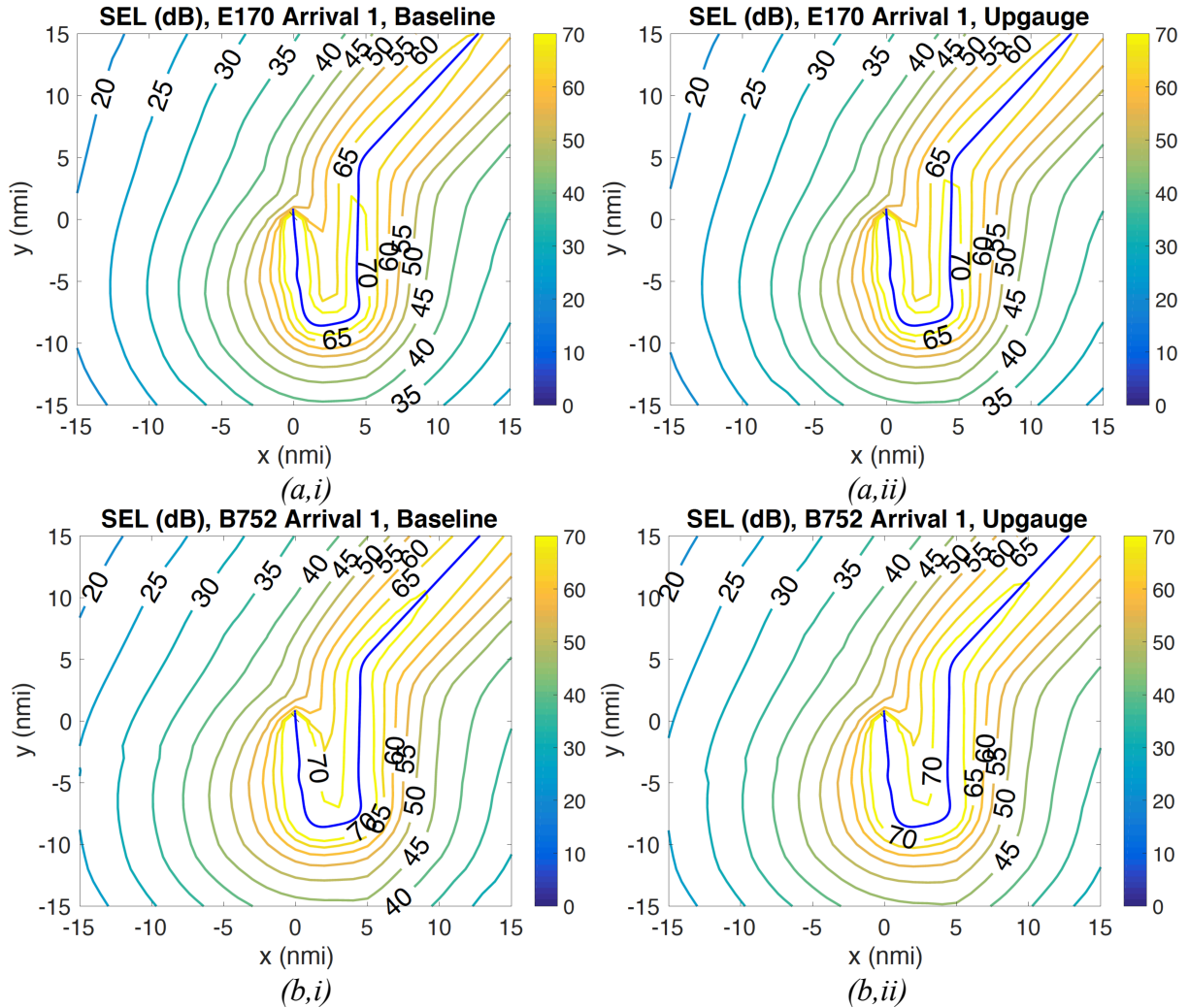
Figure 44: Sample Generated SEL Arrival Plots, E170 Baseline (a,i) and Upgauge (a,ii) on Arrival 1 & B752 Baseline (b,i) and Upgauge (b,ii) on Arrival 1

A few sample departure SEL plots for aircraft flying on departure 1 that were produced by this method are shown in *Figure 45*. In general, the upgauged aircraft departures resulted in louder SEL contours compared to their respective baseline aircraft departures. This is expected given that the upgauged aircraft are heavier, have more drag, and thus need more thrust to climb at the same rate as their baseline counterparts.
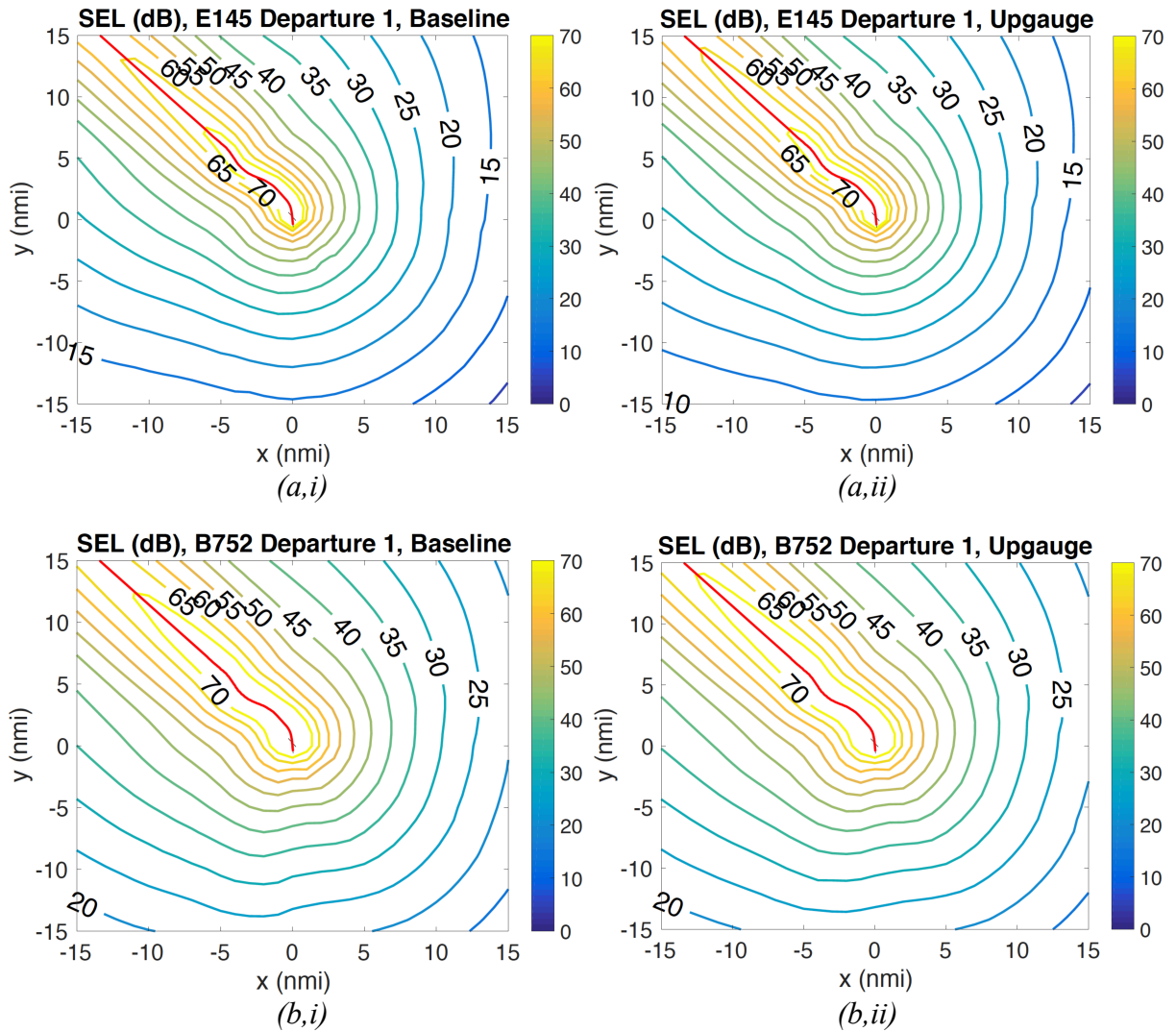
Figure 45: Sample Generated SEL Departure Plots, E145 Baseline (a,i) and Upgauge (a,ii) on Departure 1 & B752 Baseline (b,i) and Upgauge (b,ii) on Departure 1

6.5   DNL Noise Results

The final metric assessed was DNL. An SEL contour was generated for each aircraft group and gauge flying each of the four arrival tracks and six departure tracks identified in section 6.3. The total number of flights per aircraft group per day was assumed to be the average number of arrival operations of that aircraft group at DCA during all of 2015 from *Table 6* and are shown in *Table 9*. The same total percentages of each aircraft group of the average daily total were assumed to have occurred on each of the departures and arrivals.

Aircraft Group	Average Daily Total	Percentage of Average Daily Total
E170	132.4	33.47%
E145	94.8	23.97%
B738	83.6	21.13%
A320	65.9	16.67%

| MD88 | 16.6 | 4.19% |
| B752 | 2.2 | 0.56% |

Table 9: Average Daily Total Operations per Aircraft Group at DCA in 2015

The final DNL results from this analysis are shown in *Figure 46*. In general, the DNL contours of the upgauged aircraft were louder with a peak of about 0.4 dB. This is expected given that the SEL contours of the upgauged aircraft were louder for almost all flights.

(a)

(b)

(c)
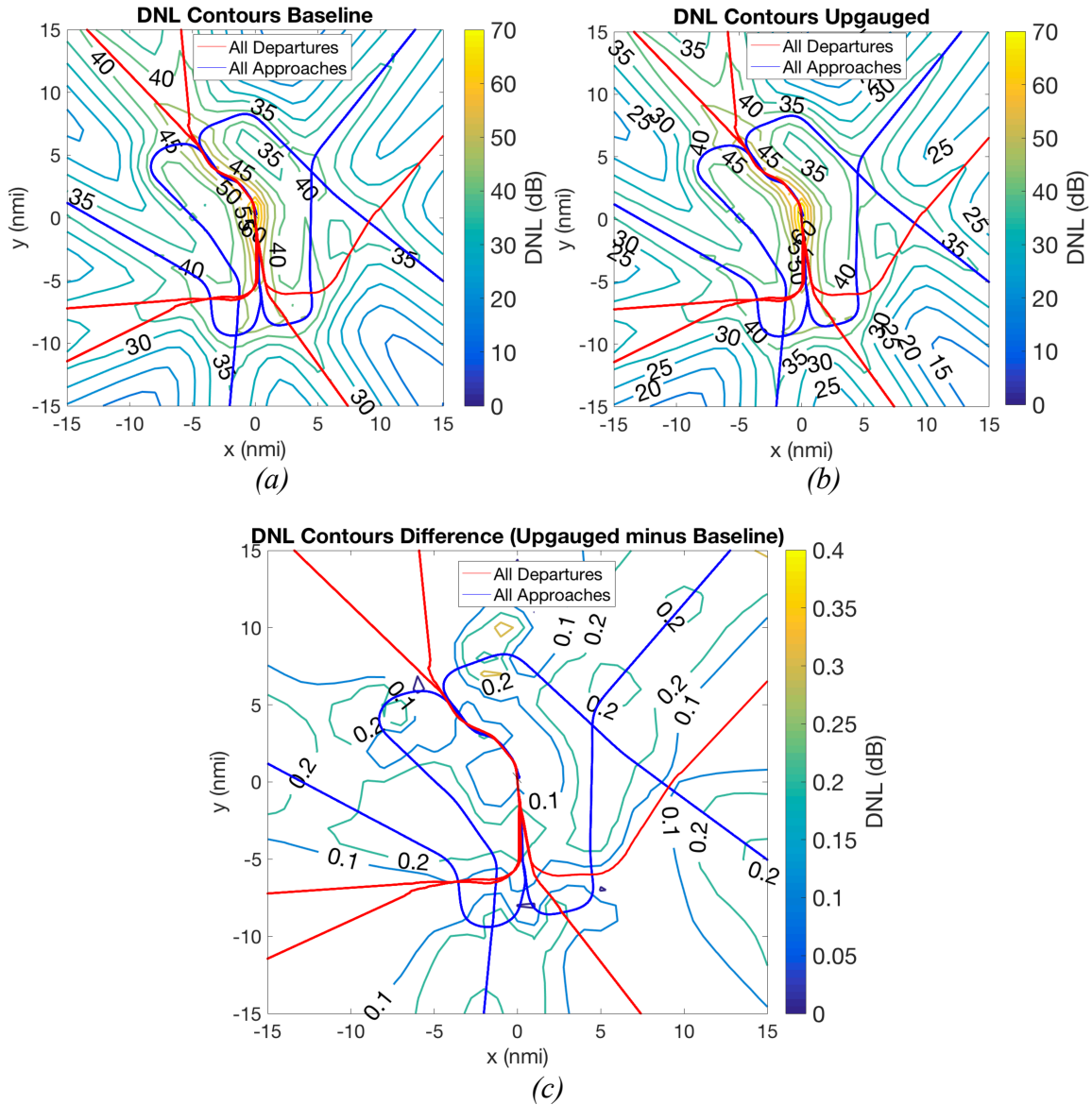
Figure 46: DNL Results, Baseline (a), Upgauge (b), & Difference (c)

6.6   Conclusion

In this case study, the noise impact of a hypothetical aircraft gauge policy implementation at DCA was examined. A baseline fleet consisting of six representative aircraft groups was modeled with a 10% increase in their fuselage length and passenger counts in TASOPT. These

baseline and upgauged aircraft were flown in the profile generator through a total of ten representative departure and arrival tracks and their SEL contours were computed in ANOPP as needed to compute DNL contours for this case. This case study is thus a good demonstrator of using the improved noise analysis method to examine the noise impacts of future aircraft, a task that cannot be completed by current noise analysis methods.

This analysis showed that with less than 0.4 increase in dB DNL at maximum for the 10% upgauged case, the noise impact of the 10% upgauged aircraft policy is small. When considering the passenger throughput through the airport for the upgauged case (25,343,000 per year versus 23,039,000 for the baseline), the increased number of passengers appears worth the small increase in noise.

Future work includes use of the improved noise analysis method in assessing the noise impact of the aircraft gauge policy at other airports or of potentially higher gauges. While upgauging in TASOPT is a relatively simple task (the aircraft's fuselage length and number of passengers merely needs to be increased by the percent gauge), the assumption that the upgauged aircraft have the same drag polars as the baseline aircraft will be less and less accurate.

7 Discussion and Conclusion

As stated at the beginning of this thesis, a noise analysis method that improves upon current noise analysis capabilities, enabling the noise modeling of advanced operational flight procedures and future aircraft designs, was designed, validated, and carried out on a couple of sample cases to show its functionality.

The improved noise analysis method addresses a shortcoming in the ability of the current noise analysis methods to assess the noise impacts of advanced operational flight procedures and future aircraft designs. Current noise analysis methods involve interpolation in thrust and distance from flight test data and assume the change in airframe noise due to configuration and speed changes negligible compared to engine noise. In order to capture the noise impacts from of advanced operational flight procedures, which sport precise changes in configuration, thrust, and speed, as well as future aircraft designs that do not yet have associated flight test data, a modeling method that computes noise at the component level using without the need for flight test data is needed. As aircraft activity continues to grow and as airframe noise becomes just as important a factor as continuously decreasing engine noise, the need to assess noise impacts of future aircraft and flight procedures becomes more and more critical.

With the improved noise analysis method, capturing the component-level noise effects of not only each major noise-producing portion of the engine individually but also the noise effects of airframe noise and specific changes in geometry and configuration is made possible by employing the tool ANOPP as its foundation. Rather than relying on a specific aircraft's flight test data for noise assessment, ANOPP is run by being supplied a set of engine performance parameters and a flight trajectory of an arbitrary aircraft, enabling flexibility in the notional aircraft and flight procedure being assessed. In order to run ANOPP efficiently with an input engine parameters and a flight profile that are physically realizable, ANOPP was combined in the improved noise analysis method with the physics-based aircraft design and optimization tool TASOPT and a flight profile generator to supply the inputs. The improved noise analysis method was validated against certification data as well as flight test data taken at Boston Logan Airport. After modeling several aircraft types and their flight procedures, the differences between the noise predictions and the recorded noise data were well within the scatter seen in typical noise measurements.

Analyzing the noise impacts of advanced operational flight procedures is made possible with the improved noise analysis method. A demonstration of this is seen in the assessment of the potential benefits or drawbacks of the delayed deceleration approach procedure, a single-event advanced operational flight procedure for which airspeed and configuration changes play a significant role in the overall aircraft noise, thus requiring the use of the improved noise analysis method since current noise analysis methods are not designed to capture these effects. In this case study, the improved noise analysis method showed that maintaining a clean configuration (and therefore lower thrust levels) but higher airspeed before waiting until the last physically possible moment to decelerate, does not necessarily serve to reduce noise in all flight position profiles if engine noise is low to begin with, such as in a continuous descent approach. This is because the high airframe noise due to maintaining a high airspeed counters the reduced noise from flying at lower thrust levels. Given this capability, further noise analysis of other advanced operational flight procedures can also be carried out given a procedure definition. Using the method to optimize a particular flight procedure for minimum noise while varying factors such

as the time of landing gear deployment, the altitude of thrust cutback, or even the aircraft flight track is another option for using this method in future work.

Finally, analyzing the noise impacts of future aircraft designs is also made possible with the improved noise analysis method. A demonstration of this is seen in the assessment of noise of a notional future aircraft fleet, a task that requires knowing the noise signatures of future aircraft. This case study showed that a sample policy implementation, where all aircraft are increased in fuselage length and payload capacity by 10%, would have a minimal impact on noise while the increase in passenger throughput is about 2 million/year. The upgauged aircraft were resized using the TASOPT component of the improved noise analysis method, which gave new performance and geometry for the aircraft fleet accordingly. Finally, ANOPP, the noise model used within the improved noise analysis method, was able to model noise given this performance and geometry data, thus removing the reliance on existing flight-test noise data to make predictions. Given this capability, this method can be used to model the noise of future aircraft that are changed beyond simple upgauging, such as aircraft with geared turbofans or aircraft with engine noise that is masked due to mounting the engines on top of the fuselage.

8 Works Cited

[1] Federal Aviaiton Administration. (2016, September) Aviation Environmental Design Tool (AEDT) Technical Manual. Electronic.

[2] Tokarev V, Attenborough K. Zaporozhets O, *Aircraft Noise : Assessment, Prediciton And Control*. New York: Spon Press, 2011.

[3] Michael J. T. Smith, *Aircraft Noise*. Cambridge, U.K.: Cambridge University Press, 1989.

[4] Antonio A. Trani. CEE 4674 Airport Planning and Design. [Online]. http://128.173.204.63/courses/cee4674/cee4674_pub/BasicNoiseCalculations.pdf

[5] Airbus, "Getting to Grips with Aircraft Noise," Flight Operations Support & Line Assistance , 2003.

[6] Jack L. Kerrebrock, *Aircraft Engines and Gas Turbines*. Cambridge, U.S.A.: MIT Press, 1984.

[7] Tokarev V, Attenborough K. Zaporozhets O, *Aircraft Noise: Assessment, Prediction, and Control*. Abington, New York: Spon Press, 2011.

[8] Airports Commission. (2013) Discussion Paper 05: Aviation Noise. [Online]. https://www.gov.uk/government/uploads/system/uploads/attachment_data/file/22376 4/airports-commission-noise.pdf

[9] Doug Irvine, "Steep Takeoffs Land JWA on 'Scariest Airports' List," *The Orange County Register* , 2012, http://www.ocregister.com/articles/john-364661-wayne-airport.html.

[10 Federal Aviation Administration. (2012, June) Greener Skies over Seattle = Greener Skies over the USA.

[11 Federal Aviation Administration. (2007, September) FAA Long-Range Aerospace Forecasts, Fiscal Years 2020, 2025 and 2030. Electronic.

[12 E. Boeker and et al., "Integrated Noise Model (INM) Version 7.0 Technical Manual," U.S. Department of Transportation Research and Innovative Technology Administration, Cambridge, 2008.

[13 J. & C. Burley Rawls, "Aircraft Noise Prediction Program (ANOPP) Tecnical Manual," NASA Langley Research Center , Hampton, 2012.

[14 M. F. Heidmann. (1979) Interim Prediction Method for Fan Compressor Source Noise. Electronic.

[15 James R. Stone and Francis J. Montegani. (1980) An Improved Prediction Method for the Noise Generated in Flight by Circular Jets. Electronic.

[16 A-21 Aircraft Noise Measure Noise Aviation Emission Modeling Committee, "Method for Predicting Lateral Attenuation of Airplane Noise," 2012.

[17 M Drela, "Transport Aircraft System OPTimization, Technical Description," Massachusetts Institute of Technology, 2011.

[18 Federal Aviation Administration. (2005, June) Advisory Circular, Aircraft Weight and Balance Control. [Online]. https://www.faa.gov/documentLibrary/media/Advisory_Circular/AC120-27E.pdf

[19 U.S. Government Publishing Office. (2017, January) Title 14 Part 25-Airworthiness

Standards: Transport Category Airplanes. [Online]. http://www.ecfr.gov/cgi-bin/text-idx?SID=6cbb4f90b0da0ab47411ccbd6a20a304&mc=true&node=sp14.1.25.b&rgn=div6#sg14.1.25.b.sg0

[20 F. Jane, *All the World's Aircraft*. London: Sampson Low, Marston, 1912.

[21 Jack L. Kerrebrock, *Aircraft Engines and Gas Turbines*, 2nd ed. Cambridge, MA, USA: The MIT Press, 1992.

[22 *IHS Jane's Aero-Engines*. Coulsdon, Surrey, UK: IHS Global Limited, 2013.

[23 A. Nuic, "User Manual for the Base of Aircraft Data (BADA) Revision 3.11," Eurocontrol, EEC Technical Report 2013.

[24 U.S. Government Publishing Office. (2016, November) Part 36-Noise Standards: Aircraft Type and Airworthiness Certification. [Online]. http://www.ecfr.gov/cgi-bin/text-idx?rgn=div5&node=14:1.0.1.3.19

[25 T. Reynolds and et al., "Delayed Deceleration Approach Noise Assessment," in *16th AIAA Aviation Technology, Integration, and Operations Conference*, Washington D.C., 2016.

[26 Federal Aviation Administration. (2012, July) Aircraft Noise Levels. Electronic.

[27 Airbus Training, "A320 Flight Crew Operating Manual, Operating Limitations," Airbus, Airbus FCOM 3.01.70.

[28 J.R. Ratley and et al., "737-600/700/800/900 Flight Crew Training Manual," Boeing Company, Boeing Company Document FCT 737 NG (TM) 2005.

[29 J.M. Dumont, "Fuel Burn Reduction Potential from Delayed Deceleration Approaches," Department of Aeronautics and Astronautics, Massachusetts Institute of Technology, Master's Thesis 2012.

[30 Metropolitan Washington Airports Authority. (2016, August) Air Traffic Statistics. Electronic.

[31 Airbus. (2015, December) A319 Aircraft Characteristics Airport and Maintenance Planning. Electronic.

[32 Airbus. (2015, May) A320, Aircraft Characteristics Airport and Maintenance Planning. Electronic.

[33 Boeing Commercial Airplanes. (2013, September) 737 Airplance Characteristics for Airport Planning. Electronic.

[34 Embraer. (2007, January) EMB145 Airport Planning Manual. Electronic.

[35 Embraer. (2008, January) EMB135 Airport Planning Manual. Electronic.

[36 (2006, June) Boeing 737 Management Reference Guide. [Online]. http://www.b737mrg.net/downloads/b737mrg_noise.pdf

[37 Federal Aviation Administration. (2015, December) AEDT Standard Input File (ASIF) Reference Guide. Document.

[38 R.H. Liebeck, "Airplane Design," Department of Mechanical and Aerospace Engineering, University of California, Irvine, Irvine,.

[39 D., et al. Raymer, "An Evaluation of Performance Metrics for High Efficiency Tube-and-Wing Aircraft Entering Service in 2030 to 2035," National Aeronautics and Space Administration, Cleveland, NASA/TM—2011-217264, 2011.

Appendix A: Assumptions and Calculation Methods to Obtain ANOPP Input Parameters within the Improved Noise Analysis Method Framework

The following explains the assumptions and methods for calculating the ANOPP input parameters in the improved noise analysis method. ANOPP requires an extensive list of input parameters that are obtained from the following sources:

1. *The Flight Profile* generated directly by the Flight Profile Generator or calculated from the Flight Profile Generator outputs;
2. *Aircraft Geometry Outputs generated by TASOPT* and used either directly by ANOPP or used after a minimal change, such as a unit conversion or normalization by another TASOPT direct output, or calculated from TASOPT outputs;
3. *Engine Performance Outputs generated by TASOPT* and used either directly by ANOPP or used after a minimal change, such as a unit conversion or normalization by another TASOPT direct output, or calculated from TASOPT outputs;
4. *Externally sourced Engine Performance or Geometry Outputs*
5. *Noise Model Control Inputs*

These parameters are boxed in red and numbered in *Figure 47*:
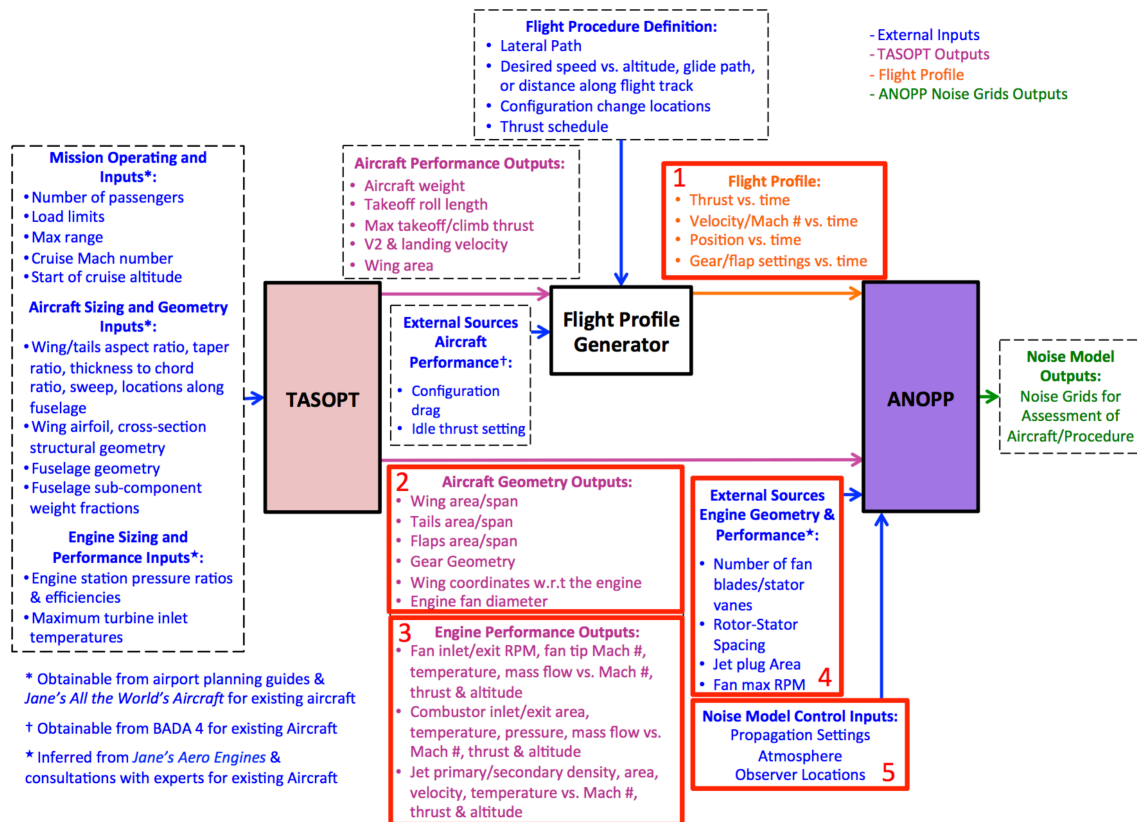
Figure 47: Improved Noise Analysis Framework, Highlighting Inputs into ANOPP & Sources

The following sections provide the detail of the conversion of TASOPT outputs, flight profile generator outputs, and information provided by user-defined external sources.

A.1 The Flight Profile

ANOPP Required Input Parameter	Direct Output from Flight Profile Generator	Post Processing to Compute ANOPP Required Input Parameter from Profile Generator Direct Output
Thrust vs. Time	Thrust vs. Time	N/A
Velocity/Mach # vs. Time	Velocity/Mach # vs. Time	N/A
Position vs. Time	Position vs. Time	N/A
Gear/flap settings vs. Time	Gear/flap settings vs. Time	N/A

Table 10: Flight Profile Parameters from the Flight Profile Generator & their Conversion to ANOPP Inputs

A.2 Aircraft Geometry Outputs Generated by TASOPT

ANOPP Required Input Parameter	Direct Output from TASOPT	Post Processing to Compute ANOPP Required Input Parameter from TASOPT Direct Output
Wing area	Wing area	N/A
Wing span	Wing span	N/A
Tail area	Tail area	N/A
Tail span	Tail span	N/A
Engine Fan Diameter	Engine Fan Diameter	N/A
Flaps area	Wing area	Flaps area = 0.3*Wing area[2]
Flaps span	Wing span	Flaps span = 0.599*Wing span[2]
Number of nose/main gear wheels	Aircraft Weight	see section A.2.1
Diameter of nose/main gear wheels	Aircraft Weight	see section A.2.1
Number of nose/main gear struts	Aircraft Weight	see section A.2.1
Length of nose/main gear struts	Engine Fan Diameter	Length of nose gear & main gear strut = Engine Fan Diameter
Wing coordinates w.r.t. the engine	Engine Fan Diameter, $\langle x,y \rangle$ position of wing along fuselage $\langle x,y \rangle$ position of engine along fuselage	see section A.2.2

Table 11: Aircraft Geometry Outputs Generated by TASOPT & their Conversion to ANOPP Inputs

A.2.1 Landing Gear Geometry

- **Number of tires and tire diameter on both the main and nose gear:**

  The number of wheels and the tire diameter of the main and nose gear are sized according to the table below using the commercial ratings column, assuming 100% take-off gross weight on the main gear and 15% on the nose gear. The lightest configuration (a combination of the number of wheels and type of tire to meet supporting strength requirements) is selected.

---

[2] These ratios correspond to that of a Boeing 737-800 [39]

Tire Size	Ply Rating	Max Width inches	Max Diam. inches	Loaded Radius inches	Tire and tube wt. lbs.	Commercial Press lbs/sq.in.	Commercial Rated Load lbs	Military Press lbs/sq.in.	Military Rated Load lbs.
24 x 7.25	10	7.3	24.0	10.3	29.7	120	6,600		
29 x 7.7	12-16	7.6	28.0	12.2	36-44	160	9,800	220	13,800
34 x 11	18	11.0	33.0	13.9	84.1	125	15,500		
36 x 11	24	11.1	35.0	15.0	86.2			220	25,600
40 x 14	22	13.5	39.2	11.8	112	145	25,000		
44 x 13	26	13.4	43.2	18.4	141.5			200	35,000
44 x 16	26	15.6	43.1	18.0	151.6	165	35,500		
56 x 16	24	16.0	55.8	24.1	258.7			178	45,000
56 x 16	32	16.1	55.8	24.1	296.3			240	60,000
56 x 16	36	16.1	55.8	24.1	297.0			280	71,000

Figure 48: Commercial and Military Landing Gear Tire Ratings, from Airplane Design, R. H. Liebeck [38]

- **Number of main and nose gear struts:**

The number of main and nose gear struts are initially assumed 2 main gear and 1 nose gear. If over 8 main gear wheels or over 4 nose gear wheels are needed using the largest diameter tires, the number of struts for either the nose or main gear is doubled and the tires are re-sized accordingly, assuming the same number of wheels on each of the main and nose gear struts

A.2.2 Wing Coordinates with Respect to Engines

The x, y coordinates of the wing on the aircraft are calculated, with the origin at the leading edge of the exposed wing root, using the wing geometry parameters provided by TASOPT and equations used in TASOPT to define the wing, shown in *Figure 49*:

$$\lambda_s = \frac{c_s}{c_o} \ , \lambda_t = \frac{c_t}{c_o}$$

$$\eta = \frac{2y}{b} \ ,$$

$$\eta_o = \frac{b_o}{b} , \eta_s = \frac{b_s}{b}$$
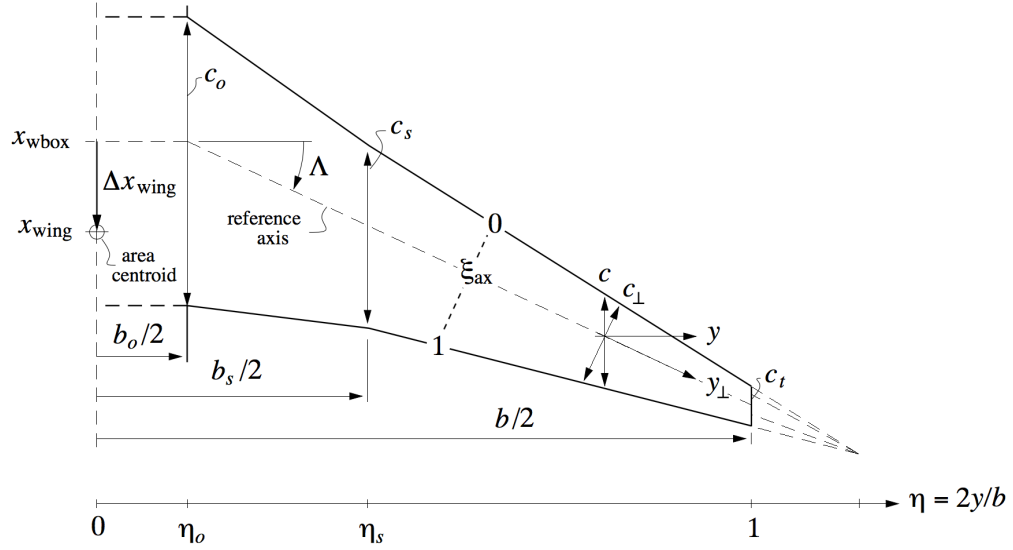
$$\frac{c(\eta)}{c_o} = C(\eta; \eta_o, \eta_s, \lambda_s, \lambda_t) = \begin{cases} 1 & , \quad 0 < \eta < \eta_o \\ 1 + (\lambda_s - 1)\dfrac{\eta - \eta_o}{\eta_s - \eta_o} & , \quad \eta_o < \eta < \eta_s \\ \lambda_s + (\lambda_t - \lambda_s)\dfrac{\eta - \eta_s}{1 - \eta_s} & , \quad \eta_s < \eta < 1 \end{cases}$$

Figure 49: Diagram of Wing Geometry used within TASOPT, from TASOPT Summary by Mark Drela [17]

$x_{wLE,r}, y_{wLE,r}$ and $x_{wLE,t}, y_{wLE,t}$, the wing root and tip leading edge x,y coordinates in the aircraft reference frame, are determined from Λ, exposed span $\frac{1}{2}(b - b_o)$, and root and tip chords c_o and c_t, and the x_{wbox} location defining the sweep reference axis.

$x_{wTE,r}, y_{wTE,r}$ and $x_{wTE,t}, y_{wTE,t}$, the wing root and tip trailing edge x,y coordinates in the aircraft reference frame, are determined by adding $c(\eta)$ to the leading edge defined coordinates at each span-wise η station

These coordinates must be converted into the reference frame of the engine, shown in *Figure 50*. Given x_{eng} and y_{eng}, the location of the engines in the aircraft reference frame, and by assuming that the center of the engines are one engine radius above (for fuselage mounted engines) or below (for wing mounted engines) the wing plane (neglecting the aircraft wing's dihedral), the coordinates of the wing with respect to the engines is finally determined.

$$x_{wLE,rE} = x_{eng} - x_{wLE,r}$$

$$y_{wLE,rE} = y_{eng} - y_{wLE,r}$$

$$x_{wLE,tE} = x_{eng} - x_{wLE,t}$$

68

$$y_{wLE,tE} = y_{eng} - y_{wLE,t}$$

$$x_{wTE,rE} = x_{eng} - x_{wTE,r}$$

$$y_{wTE,rE} = y_{eng} - y_{wTE,r}$$

$$x_{wTE,tE} = x_{eng} - x_{wTE,t}$$

$$y_{wTE,tE} = y_{eng} - y_{wTE,t}$$

$$z_{wLE,rE} = z_{wLE,tE} = z_{wTE,rE} = z_{wTE,tE} = \begin{cases} 0.5d_{fan}, & \text{Fuselage Mounted Engines} \\ -0.5d_{fan}, & \text{Wing Mounted Engines} \end{cases}$$
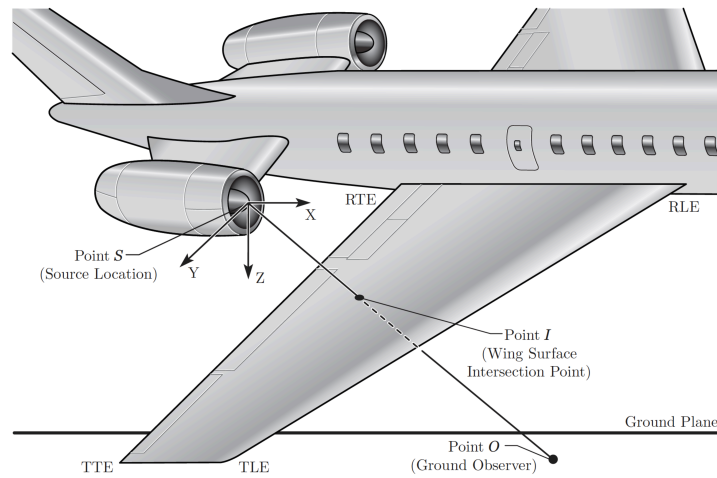
Figure 50: Diagram of Engine Coordinate System used within ANOPP [13]

A.3 Engine Performance Outputs Generated by TASOPT

ANOPP Required Input Parameter[3]	Direct Output from TASOPT	Post Processing to Compute ANOPP Required Input Parameter from TASOPT Direct Output
Fan inlet RPM	N1, the fan rotation rate percentage of the maximum fan RPM	Fan inlet RPM = N1*Fan Max RPM[4]
Fan Relative Tip Mach Number	see section A.3.1	see section A.3.1
Fan Inlet Total Temperature	Fan Inlet Total Temperature	N/A
Fan Exit Total Temperature	Fan Exit Total Temperature	N/A
Fan Inlet Mass Flow Rate	Core Mass Flow Rate, Bypass Ratio (BPR)	Fan Exit Mass Flow Rate = (BPR+1)*Core Mass Flow Rate
Fan Exit Mass Flow Rate	Core Mass Flow Rate, Bypass Ratio (BPR)	Fan Exit Mass Flow Rate = BPR*Core Mass Flow Rate
Combustor Inlet Total Temperature	Combustor Inlet Total Temperature	N/A
Combustor Exit Total Temperature	Combustor Exit Total Temperature	N/A
Combustor Inlet Total Pressure	Combustor Inlet Total Pressure	N/A
Combustor Exit Total Pressure	Combustor Exit Total Pressure	N/A
Combustor Mass Flow Rate	Core Mass Flow Rate	N/A
Combustor Area	see section A.3.1	see section A.3.1
Jet Primary Stream Density	see section A.3.1	see section A.3.1
Jet Secondary Stream Density	see section A.3.1	see section A.3.1
Jet Primary Stream Area	Jet Primary Stream Area	N/A
Jet Secondary Stream Area	Jet Secondary Stream Area	N/A
Jet Primary Stream Velocity	Jet Primary Stream Velocity	N/A
Jet Secondary Stream Velocity	Jet Secondary Stream Velocity	N/A
Jet Primary Stream Total Temperature	see section A.3.1	see section A.3.1
Jet Secondary Stream Total Temperature	see section A.3.1	see section A.3.1

Table 12: Engine Performance Outputs Generated by TASOPT & their Conversion to ANOPP Inputs

A.3.1 Conversion of Engine Performance Outputs from TASOPT to ANOPP Inputs

TASOPT outputted parameters are collected at the stations shown in the engine diagram shown in *Figure 51* at several thrust, Mach number, and altitude operating points. The parameters highlighted below are used to perform the final conversions of the remaining

---

[3] All of these parameters are needed as a function of thrust, ambient Mach number, and altitude

[4] See section A.4, which describes where this parameter is obtained

TASOPT output engine performance parameters to ANOPP input parameters that were not yet explained in *Table 12*.

(a)

```
B2: alt.   =    8375. ft
B2: Mach   =   0.4713
B2: BPR    =   5.0970
B2: N1     =   1.0635
B2: Feng   =  62.051    kN
B2: mcore  =  50.867    kg/s

B2: loc      Tt       pt       cpt       R      cpt/(cpt-R)
             K        kPa      J/kg K    J/kg K
      0     283.6    86.24    1008.7    288.3    1.4002
      2     283.6    85.81    1008.7    288.3    1.4002
     21     331.8   141.46    1011.1    288.7    1.3989
      7     331.8   138.63    1011.1    288.3    1.3989

      0     283.6    86.24    1008.7    288.3    1.4002
     18     283.6    85.81    1008.7    288.7    1.4002
     19     283.6    85.81    1008.7    288.7    1.4002
     25     378.9   214.14    1014.9    288.7    1.3968
      3     815.1  2565.67    1105.6    288.3    1.3527
      4    1509.0  2411.73    1265.7    288.8    1.2956
     41    1423.0  2256.59    1248.5    288.7    1.3008
     45    1052.3   547.08    1189.6    288.7    1.3205
     49     759.9   128.63    1122.2    288.7    1.3464
      5     759.9   127.99    1122.2    288.7    1.3464

B2: loc      T        p        M        u        A       Fsp      eta_p
             K        kPa               m/s      m^2
      0     271.6    74.12   0.4713   155.66   2.0943   0.6058
      2     264.6    67.31   0.5993   195.87   1.7944

     25     353.5   167.76   0.6013   226.98   0.1361

      5     659.2    74.12   0.9300   472.74   0.2810
      6     659.2    74.12   0.9300   472.74   0.2810   0.1615   0.4954

      7     277.5    74.12   0.9896   331.18   0.8448
      8     277.5    74.12   0.9896   331.18   0.8448   0.4443   0.6395
```

(b)

Figure 51: Turbofan Engine Layout Used in TASOPT's Engine Calculations [17] *(a) & Example Table of TASOPT's Engine Performance Outputs at Each Station of a Sample Engine at One Specific Mach Number, Thrust, and Altitude Operating Point (b)*

- d_{Fan}: Fan diameter
- N_1: Fan normalized rotational speed
- BPR: Bypass ratio
- $\dot{m}_{core}$: Core mass flow
- M_2: Mach number at station 2
- M_{25}, T_{t25}: Mach number and Total Temperature at station 25
- p_{t3}, T_{t3}: Total pressure, total temperature at station 3
- T_6, A_6, M_6, u_6: Static temperature, area, Mach number, velocity at station 6 as a function of Mach Number, Thrust, and Altitude
- T_8, A_8, M_8, u_8: Static temperature, area, Mach number, velocity at station 8 as a function of Mach Number, Thrust, and Altitude
- $RPM_{fan,max}$: Maximum fan RPM

- **Fan Rotor Relative Tip Mach Number M$_D$:**

$$M_t = \pi d_{fan}(RPM_{fan,max}N_1)\left(\frac{1+0.2M_2^2}{\gamma RT_{t2}}\right)^2 10$$

$$\boldsymbol{M_D} = \left(M_t^2 + M_2^2\right)^{1/2}$$

- **Area at Combustor Inlet/Exit:**

$$M_{25}\sqrt{\frac{T_{t25}}{(1+0.5(\gamma-1)M_{25}{}^2)}} = M_3\sqrt{\frac{T_{t3}}{(1+0.5(\gamma-1)M_3{}^2)}} => solve\ for\ M_3$$

$$T_3 = T_{t3}/(1+0.5(\gamma-1)M_3{}^2)$$

$$p_3 = p_{t3}/(1+0.5(\gamma-1)M_3{}^2)^{\gamma/\gamma-1}$$

$$A_{combustor} = \frac{\dot{m}_{core}}{M_3\sqrt{\gamma RT_3}\frac{p_3}{RT_3}}$$

- **Total temperature of Jet Primary/Secondary Stream:**

$$\boldsymbol{T}_{tjet,primary} = T_6(1+0.5(\gamma-1)M_6{}^2)$$

$$\boldsymbol{T}_{tjet,secondary} = T_8(1+0.5(\gamma-1)M_8{}^2)$$

- **Density of Jet Primary/Secondary Stream:**

$$\boldsymbol{\rho}_{jet,primary} = \frac{\dot{m}_{core}}{A_6 u_6}$$

$$\boldsymbol{\rho}_{jet,secondary} = \frac{BPR\dot{m}_{core}}{A_8 u_8}$$

A.4 Externally Sourced Engine Performance and Geometry Outputs

ANOPP Required Input Parameter	Direct Engine Geometry and Performance Input	Post Processing to Compute ANOPP Required Input Parameter from Direct Geometry and Performance Input
Number of Fan Blades	Number of Fan Blades[5]	N/A
Number of Stator Vanes	Number of Stator Vanes[5]	N/A
Rotor-Stator Spacing	Rotor-Stator Spacing[5]	N/A
Jet Plug Area	Jet Plug Area[5]	N/A
Max Fan RPM	Max Fan RPM[5]	N/A

Table 13: Externally Sourced Engine Performance and Geometry Outputs & their Conversion to ANOPP Inputs

---

[5] Typically obtained from *Jane's Aero-Engines* [22] for existing aircraft types

A.5 Noise Model Control Input Parameters

ANOPP Required Input Parameter	Direct Noise Model Control Input	Post Processing to Compute ANOPP Required Input Parameter from Direct Noise Model Control Input
Ambient speed of sound per time	Ground level temperature[6]	see section A.5.1
Ambient density per time	Ground level temperature, pressure[6]	see section A.5.1
Ambient dynamic viscosity per time	Ground level temperature, dynamic viscosity[6]	see section A.5.1
Ambient absolute humidity per time	Ground level temperature, pressure, relative humidity[6]	see section A.5.1
Observer x,y,z grid	Observer x,y,z grid	N/A
Flag to compute atmospheric attenuation effects	Flag to compute atmospheric attenuation effects[7]	N/A
Flag to compute ground effects	Flag to compute ground effects[8]	N/A
Flag to indicate type of surface to be used in calculating ground effects (hard or soft)	Flag to indicate type of surface to be used in calculating ground effects (hard or soft) [9]	N/A

Table 14: Noise Model Control Input Parameters & their Conversion to ANOPP Inputs

A.5.1 Ambient atmospheric parameters per time in the aircraft flight profile

Ground level temperature T_A and pressure p_A are used to compute the ambient temperature and pressure with altitude in the aircraft flight profile per time. These are used to compute the remaining atmospheric parameters with time in the aircraft flight profile:

Ambient temperature per time:

$$T_0(t) = \begin{cases} T_A - z(t)lapse, & z(t) < 37000ft \\ 216.65\ K, & z(t) \geq 37000ft \end{cases}$$

Normalized ambient temperature[10] per time:

$$T_0(t)^* = \frac{T_0(t)}{T_A}$$

---

[6] Standard day atmospheric conditions assumed on default

[7] Set to "on" on default

[8] Set to "on" on default

[9] Set to "soft" on default

Ambient pressure per time:

$$p_0(t) = p_A e^{\frac{gz(t)}{-RT_A}}$$

Normalized ambient pressure[10] per time:

$$p_0(t)^* = \frac{p_0(t)}{p_A}$$

- **Ambient speed of sound per time:**

$$c_0(t) = \sqrt{\gamma R T_0(t)}$$

- **Ambient air density per time:**

$$\rho_0(t) = \frac{p_0(t)}{R T_0(t)}$$

- **Ambient air dynamic viscosity[10] per time (function of ground level dynamic viscosity μ_A):**

$$\mu_0(t) = \frac{\mu_A(1.38313 T_0(t)^{*1.5})}{T_0(t)^* + 0.38313}$$

- **Ambient absolute humidity[10] per time (function of ground level relative humidity h_A):**

$$h_0(t) = \frac{h_A}{p_0(t)^*}\left(10^{8.4256 - \left(\frac{10.1995}{T_0(t)^*}\right) - 4.922\log_{10}(T_0(t)^*)}\right)$$

[10] Equations taken from *Aircraft Noise Prediction (ANOPP) Theoretical Manual* [13]